Report

Daniel Cantero

Strain-based structural health monitoring of post-tensioned bridge

Herøy FoU: WP1 activities and results report

Trondheim – January – 2025

NTNU
Norwegian University of Science and Technology
Faculty of Engineering
Department of Structural Engineering

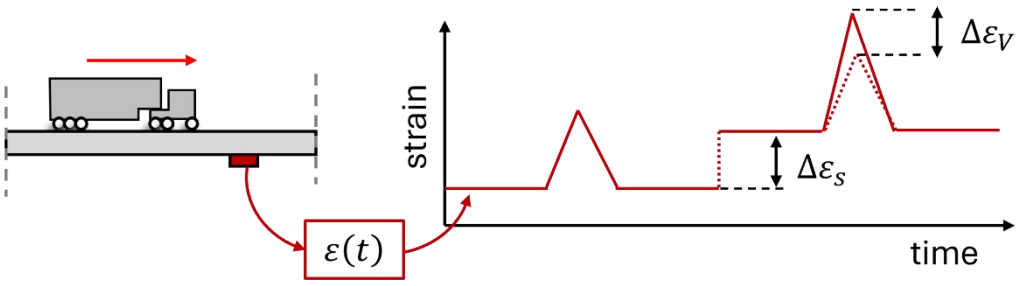

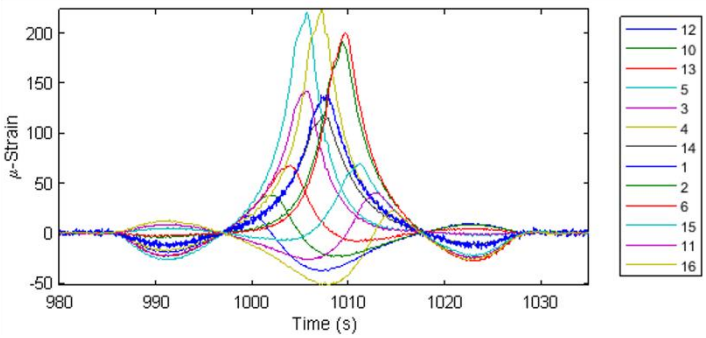

NTNU
Norwegian University of Science and Technology

Report

Strain-based structural health monitoring of post-tensioned bridge

Herøy FoU: WP1 activities and results report

VERSION
1

DATE
January 2025

AUTHOR
Daniel Cantero

PROJECT NUMBER
986917104
Cristin-project-ID: 2561686

CLIENT(S)
Nordland Fylkeskommune
Statens Vegvesen

NUMBER OF PAGES
64

ABSTRACT

This document reports the activities related to work package (WP1) of the Herøy FoU project. The work package focuses on Structural Health Monitoring (SHM), in particular using strain signals. The work within this work package has been divided into four distinct activities:

- WP1.A1 Installation of additional sensor system. Activity to extend the number of sensors on the existing instrumentation.
- WP1.A2 Calibration runs. Perform controlled traffic loading events to correlate the responses to the known weights.
- WP1.A3 Master thesis works. Supervise the work of NTNU students towards a master thesis focusing on various aspects of the problem, such as simulation, structural analysis and signal processing.
- WP1.A4 Reporting. Gather all results from master thesis works together with additional investigations as a result of the activities in WP1.

This document describes these activities in separate chapters, offering a comprehensive summary of each, along with additional investigations that complement the findings. It concludes with a discussion section, followed by the conclusions and recommendations drawn from the work conducted.

REPORT NUMBER
WP1.A4.NTNU.Report

CLASSIFICATION
Open

Preface and acknowledgements

The work presented in this document has been funded by Nordland Fylkeskommune (NFK) and Statens Vegvesen (SVV). These outcomes are part of the Herøy FoU research project, spanning from 2022 to 2024.

Table of contents

1. Introduction

Monitoring has proven to be effective in assessing the structural integrity of bridges, as demonstrated by the monitoring of the Stavå Bridge [1]. Standard continuous monitoring typically involves measuring the dynamic response of the structure, most commonly through acceleration measurements. However, research has shown that certain types of damage, such as the loss of prestressing force, do not significantly affect the dynamic properties of the structure. Specifically, frequencies remain largely unchanged despite the loss of prestressing force, as noted in previous studies [2]. This issue has been further investigated by others, such as [3], which clarified that changes in frequency can only be observed if the loss of prestressing force results in opening or closing cracks, thus altering the stiffness of the affected sections. However, even in these cases, the changes in stiffness may be minimal, leading to only marginal alterations in dynamic properties, such as frequencies.

Instead, the loss of prestressing force or tendon breakage tends to manifest more prominently in the static components of the structure. This study focuses on exploring the potential of using strain-based continuous measurements as a method for detecting such damage. The primary goal is to investigate the feasibility of an early warning system for bridge structural safety, specifically aimed at detecting sudden changes in the bridge's response, such as tendon breakage.

The starting point for this work package (WP) is the utilisation of the existing monitoring installation on the bridge. This installation has been extended by adding more sensors, specifically strain gauges, to improve the monitoring capabilities. The installation will be calibrated to ensure accurate readings. The signals collected from these sensors will be used to assess the vehicle load on the structure. A methodology has been developed to identify potential indications of damage based on the sensor data. In addition, this work is supported by numerical studies to investigate the detectable effects of damage, should such events occur, enhancing the understanding of how damage impacts the bridge's response.

The activities reported here are part of work package WP1, which focuses on Structural Health Monitoring (SHM) for the Herøy FoU project. The task within this work package has been divided into four distinct activities:

- WP1.A1 Installation of additional sensor system. Activity to extend the number of sensors on the existing instrumentation.
- WP1.A2 Calibration runs. Perform controlled traffic loading events to correlate the responses to the known weights.
- WP1.A3 Master thesis works. Supervise the work of NTNU students towards a master thesis focusing on various aspects of the problem, such as simulation, structural analysis and signal processing.
- WP1.A4 Reporting. Gather all results from master thesis works together with additional investigations as a result of the activities in WP1.

This document describes these activities in separate chapters, offering a comprehensive summary of each, along with additional investigations that complement the findings. It concludes with a discussion section, followed by the conclusions and recommendations drawn from the work conducted.

1.1. Strain-based monitoring concept

The main objective is to utilise continuously measured strain to detect tendon breakage, as illustrated in Figure 1. The continuous strain records should exhibit distinct features that indicate whether damage has occurred. Additionally, the data from the monitoring system should offer insights into the location, extent, and magnitude of the damage.

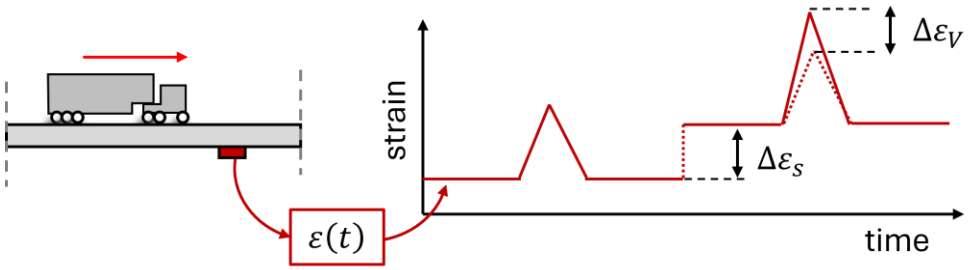

Figure 1: Strain-based monitoring concept

To develop such a system, we must first define the effect of tendon breakage. This is a complex issue influenced by factors such as the presence of voids in the duct, the condition of the grout, and the cross-sectional properties of the structure. In general, a generic post-tensioned element can be defined, as shown in Figure 2(a). The active steel is located within a grouted duct, and there may be regions with missing grout (voids) or poor grout quality. The corrosion of the tendon leads to a reduction in the steel area, which can eventually cause tendon breakage, as depicted in Figure 2(b). At the location of the breakage, the area of active steel becomes zero ($A_P = 0$). The effect of this breakage is determined by the length of the void (or poor grout region) L_{void}, as well as the transmission length L_T on both sides of the damage.

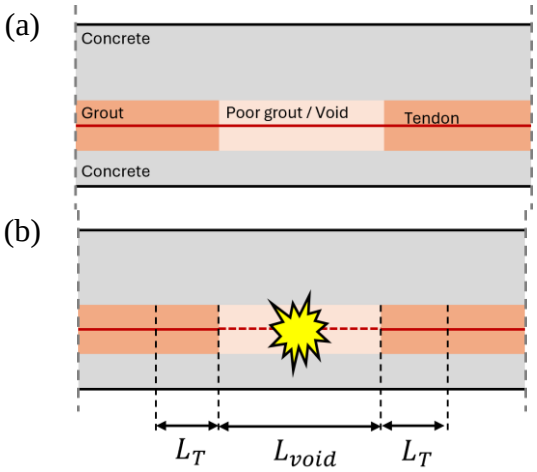

Figure 2: (a) Schematic representation of grouted post-tensioned element with poor grout/void; (b) Damage variables definition

The main effect of tendon breakage is the loss of prestressing force along the affected length. The extent of this loss depends on the length of the void and the condition of the grout. Once the steel is surrounded by healthy grout again, the prestressing force gradually increases from zero to its maximum value over a certain length, known as the transmission length (L_T). Therefore, the prestressing force along the structure can be schematically represented, as shown in Figure 3(a). For practical analysis and calculations, this can be simplified to the model shown

in Figure 3(b), which provides a more straightforward way of assessing the effect of tendon breakage on the structure.

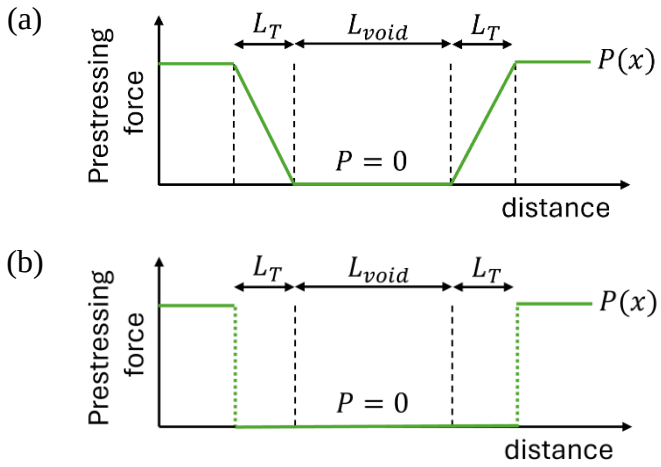

Figure 3: (a) Schematic representation of prestressing force magnitude around the tendon breakage; (b) Simplification of the prestressing force magnitude.

Another effect of the breakage is a small reduction in the cross-section's bending stiffness along the affected areas. However, the effect of this is small because the area of a tendon is relatively very small compared to the area of concrete. In addition, the effect of this variation depends on the bonding condition and the reduction in bending stiffness is difficult to quantify when the tendon is unbonded or partially bonded such as in cases with voids or poor grout in the duct.

With this framework, the continuous strain signal measured at a location on the bridge can be described by the equation in Eq. (1), as illustrated in Figure 1. The static component of the strain signal, denoted as ε_s, may change over time due to operational variations, such as sensor drift, and ambient loading effects, such as temperature fluctuations. When a vehicle passes, it induces a momentary strain variation, denoted as ε_V, which is superimposed onto the underlying strain signal.

$$\varepsilon(t) = \varepsilon_s(t) + \varepsilon_V(t) + \Delta\varepsilon_s + \Delta\varepsilon_V(t) \qquad \text{Eq. (1)}$$

When damage occurs in the form of tendon breakage, both components of the strain signal will be affected. The change in the static strain, $\Delta\varepsilon_s$, represents a permanent shift that will add a constant value to the recorded signal. Additionally, damage may alter how the structure responds to traffic loads, leading to a variation in the vehicle load related component, denoted as $\Delta\varepsilon_V$.

When damage occurs, the change in static strain ($\Delta\varepsilon_s$) is non-zero, which should be clearly detectable in the measured signal as a sudden jump. In contrast, the impact on the structure's response to traffic loading depends on the structural configuration. For statically determinate structures, the change in dynamic strain ($\Delta\varepsilon_V$) is zero because strain is directly proportional to the bending moment, and this remains unaffected by the bending stiffness. However, an exception arises if the sensor is located precisely at the damaged section, where the signal might reflect a change in bending stiffness at that specific section. In statically indeterminate

structures, the effect of damage is generally not zero ($\Delta\varepsilon_V \neq 0$), regardless of the sensor's location or the section being measured.

It is already known that the change in the static component ($\Delta\varepsilon_s$) is generally greater than the change in the vehicle response ($\Delta\varepsilon_V$), meaning $\Delta\varepsilon_s > \Delta\varepsilon_V$. One approach to amplify the effect of the vehicle response variation for damage detection is to consider the entire duration of the vehicle crossing event. Since the vehicle's Gross Vehicle Weight (GVW) is proportional to the integral of the measured strain response (Eq. (2)), this relationship can be used to enhance the detection of tendon breakage. Instead of relying on a single sample to quantify the variation, this method accumulates the changes over the entire duration of the vehicle crossing, which can magnify the effect of the damage and potentially make it more detectable.

$$GVW \propto \int \varepsilon(t)\, dt \qquad \text{Eq. (2)}$$

Therefore, this work will explore the feasibility of detecting a damaged tendon by analysing the measured strain responses. By examining the changes in both the static and vehicle components of the strain signal, and considering the full duration of vehicle crossings, the study aims to develop a potential method for identifying tendon breakage in post-tensioned structures.

2. New instrumentation

The first task in this work package involved extending the existing instrumentation on the bridge. The original installation consisted of 6 strain gauges, 2 crack width measurement sensors, and 1 temperature sensor. The new installation added 7 additional strain gauges. A detailed description of both the existing and newly installed sensors can be found in [4], which were installed and delivered by HBK/HBM.

The new system was defined by practical and economical constraints. The existing installation had 7 empty channels, and the sensor locations were chosen on the main span, where the carbon fibre plate was situated, due to the proven good results from the initial 6 strain gauges. Table 1 shows the final system, including the updated sensor information. This is an amended version compared to [4], with revised naming conventions and values. The table provides the sensor number corresponding to the channel number in the system, and both names are used interchangeably throughout this document. Additionally, HBM adopted a naming convention, as shown in the table, which varies depending on the installation phase.

Table 1: Sensor information

Sensor Num. (Channel ID)	Name	Installation date	Type	Mounted on beam	Distance to centre (mm)
1	Point_1_N	Sept. 2020	Strain	North	+ 640
2	Point_2_N	Sept. 2020	Strain	North	+ 5 120
3	Point_3_N	Sept. 2020	Strain	North	− 5 300
4	Point_4_S	Sept. 2020	Strain	South	− 940
5	Point_5_S	Sept. 2020	Strain	South	− 5 390
6	Point_6_S	Sept. 2020	Strain	South	+ 5 960
7	Omega_N	Sept. 2020	Crack width	North	+ 5 120
8	Omega_S	Sept. 2020	Crack width	South	+ 5 960
9	PT100_Temp	Sept. 2020	Temperature	North	+ 70 000
10	Point_N+1500	May 2023	Strain	North	− 15 000
11	Point_N-1500	May 2023	Strain	North	+ 15 000
12	Point_S+2000	May 2023	Strain	South	− 20 000
13	Point_S+1000	May 2023	Strain	South	− 10 000
14	Point_S+0	May 2023	Strain	South	0
15	Point_S-1000	May 2023	Strain	South	+ 10 000
16	Point_S-2000	May 2023	Strain	South	+ 20 000

Figure 4 shows a schematic map of all the strain sensor locations. Note that the locations are not drawn to scale. The reference system is defined at the mid-span of the central span of the Herøysund Bridge, with positive values indicating the direction towards the East.

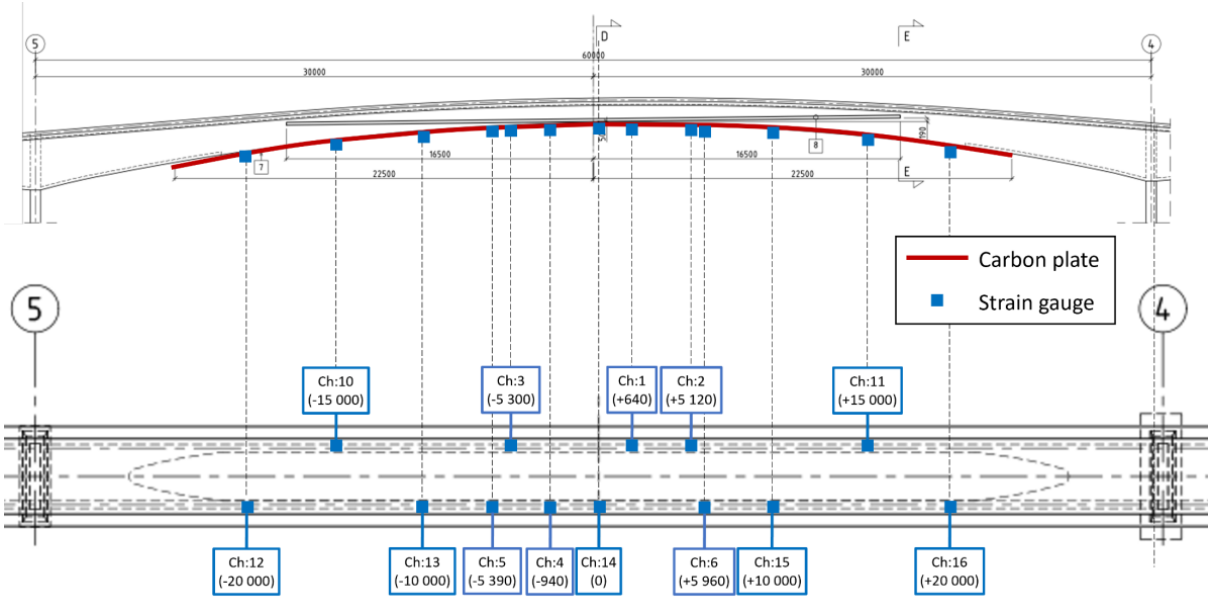

Figure 4: Map of strain gauges, with their channel number and distance to the centre of the bridge in mm (drawing not to scale).

Figure 5(a) shows the cabinet containing all the instrumentation equipment, data logging system, and local PC. It highlights that all channels in the data logger (module with large black X) are fully occupied, with no empty channels. The figure also provides an example of a strain gauge installed on the soffit of the bridge (Figure 5(b)), attached to the carbon fibre plate and protected by a cover and paint.

It is important to note that all strain gauges were equipped with temperature compensation. To achieve this, an additional unattached strain gauge was included to measure the effect of temperature on the sensor. This temperature effect is then subtracted from the sensor measuring the bridge response, ensuring that the recorded signal reflects the pure bridge behaviour. While the bridge behaviour is influenced by temperature, this strategy effectively removes the bias produced by the sensor itself.

(a) (b)

Figure 5: (a) Cabinet with logging equipment showing all channels under use
(b) Example of one strain gauge installation (Sensor 12)

The signals are stored locally using Catman software [5], and data saved in files containing 1-hour measurements. The signals are stored locally on the PC, which could be accessed remotely using TeamViewer. The file system consists of a *.tst* file, which contains auxiliary information for the system, and a *.bin* file, which holds the signals. The *.bin* files contain all the signals and timestamps for one hour of data. Each *.bin* file also includes additional information about the status of the measurement system. All signals are sampled at 20 Hz, and the typical size of a *.bin* file is approximately 6228 kB for 9 sensors and 10188 kB for 16 sensors. These *.bin* files can be processed using Catman software [5], a proprietary software from HBK. Alternatively, they can be opened and processed using the Python library apread 1.1.3 [6].

2.1. Monitoring period

For this study, all relevant signals were copied and analysed. Data collection spans from 15th September 2020 to 30th September 2024. Although the system continues to log signals beyond this period, no additional data was retrieved for the purposes of this work.

Throughout the extended measurement period, various challenges arose, including changes in sensor configuration, system errors, corrupted files, power outages, and unresponsive systems. Despite these practical difficulties, the signals were carefully cleaned to ensure data quality. Files were excluded if they exhibited: changes in the order of sensors, excessive or insufficient duration, sampling periods different from 50 ms (20 Hz). After this filtering process, a total of 30 406 files remained, each containing one hour of recorded signals. Measurements taken up to May 2023 included data from nine sensors, while files recorded thereafter captured signals from 16 sensors.

To provide a clear overview of the monitoring system's data availability, Figure 6 illustrates the status of recorded information for each month and channel. The figure represents the entire dataset with 30 406 dots corresponding to the one-hour signals for each channel. Here, black dots indicate valid signals that meet the required criteria and are usable for analysis. Red dots signify periods when the respective sensor was non-functional or broken, while white gaps represent intervals primarily caused by power outages or files with incorrect characteristics, such as corrupted data or improper configuration. This visualization highlights the operational periods of the system and the data quality over time.

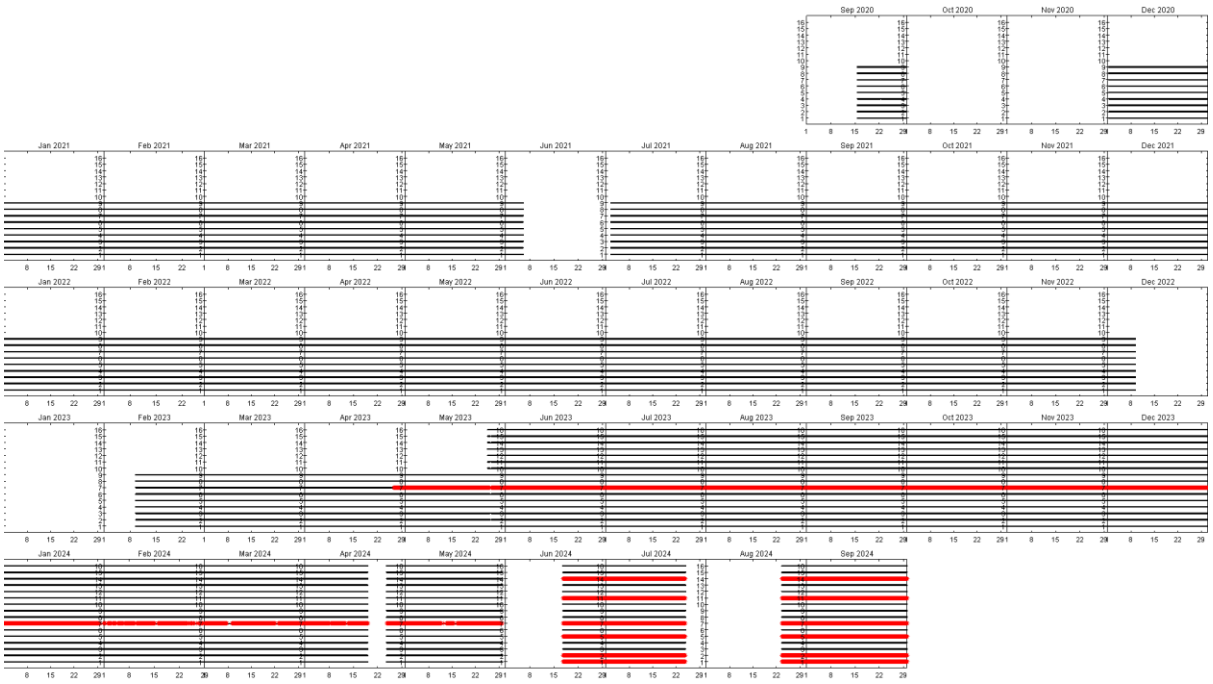

Figure 6: Overview of available data for each channel. Black = Available; Red = Broken; Missing = unavailable, corrupted or not valid.

The initial system installation occurred in early September 2020, but the sampling rate was initially set very high. By mid-September 2020, the system was adjusted to the standard rate of 20 Hz, which marks the starting point of the usable database. However, several issues and changes occurred throughout the monitoring period, including other sampling rate adjustments, power outages, and sensor malfunctions:

- October–November 2020: The sampling frequency was reduced temporarily, leading to the removal of these files from the database.
- Power outages: Resulted in data gaps during the following periods:
    - Early June to early July 2021
    - Mid-December 2022 to mid-February 2023
    - One week in April 2024
    - Two weeks in June 2024
    - Late July to late August 2024
- Sensor updates and failures:
    - Late April 2023: Sensor 7 (crack width) stopped functioning.
    - Late May 2024: Seven additional strain sensors were installed, increasing the total from 9 to 16 channels.
    - Post-June 2024 outage: Several sensors (1, 2, 5, 7, 11, and 14) stopped functioning. Despite remote and on-site investigations, no evident cause for this malfunction was identified. Without direct access to the sensors, repairs were not feasible.

3. Strain calibration

The calibration process involved monitoring the passage of heavy trucks under controlled conditions. For each calibration event, a single truck crossed the bridge at a constant speed. Temporary traffic regulations ensured that no other vehicles were present on the bridge during these events. The axle weights and dimension of the trucks used were measured beforehand. This calibration was repeated on 3 different days. Table 2 provides a summary of relevant information for each calibration day. Note that the total Gross Vehicle Weight (GVW), is provided in kilonewtons (kN).

Table 2: Calibration events summary

Calibration Day	Date	Number of events	GVW (kN)
1	13th September 2023	12	290.0
2	30th April 2024	8	462.8
3	13th September 2024	12	259.1

The calibration process involves collecting strain signals as trucks cross the bridge and using this data to extract the vehicle's speed. By converting the signal into the space domain, the area under the strain signal curve can be calculated. This area is then correlated with the known Gross Vehicle Weight (GVW) of each truck to determine a calibration factor. This factor is specific to each sensor, reflecting the unique response characteristics of their locations. Furthermore, it was observed that the calibration factor is not constant but varies depending on the load level, highlighting a non-linear relationship between the measured signal and the applied weight.

3.1. Calibration runs

3.1.1. Calibration Day 1

The first calibration session was performed on 13th September 2023, using a 3-axle Scania R164GA6X4NA truck loaded with gravel, depicted in Figure 7. During this test, the truck traversed the bridge at predefined speeds of 10 km/h, 20 km/h, and 30 km/h. The driver was instructed to maintain a constant speed throughout each crossing. These controlled conditions were essential for accurately correlating the strain signal with the vehicle's Gross Vehicle Weight (GVW) during calibration.

Table 3 provides detailed information about the truck used during Calibration Day 1. The axle spacing indicates the distance between each axle and the preceding one, while the axle distance represents the cumulative total of these spacings. The axle distance of the rearmost axle is often referred to as the wheelbase of the vehicle.

Table 3: Properties of Day 1 calibration truck

Axle number	Axle weigth (kN)	Axle spacing (m)	Axle distance (m)
1	100.0	-	0
2	95.0	3.500	3.500
3	95.0	1.355	4.855
Total	290.0	-	-

Figure 7: Day 1 calibration truck

Table 4 presents detailed information about each calibration event. The events are categorized based on the direction of travel, with directions labelled as East or West. For reference, the west end of the bridge corresponds to the side nearest the supermarket. For each event, the table includes the filename containing the corresponding signals, along with the approximate start and end times that delimit the event.

Table 4: Events for Day 1 calibration

Event number	Dir.	Vel. (km/h)	File name	Start time (s)	End time (s)
1	W-E	10	2023\09\Data_732.BIN	980	1035
2	E-W	10	2023\09\Data_732.BIN	1130	1190
3	W-E	20	2023\09\Data_732.BIN	1270	1305
4	E-W	20	2023\09\Data_732.BIN	1405	1440
5	W-E	30	2023\09\Data_732.BIN	1490	1515
6	E-W	30	2023\09\Data_732.BIN	1615	1640
7	W-E	10	2023\09\Data_732.BIN	1695	1752
8	E-W	10	2023\09\Data_732.BIN	1870	1930
9	W-E	20	2023\09\Data_732.BIN	1980	2015
10	E-W	20	2023\09\Data_732.BIN	2090	2125
11	W-E	30	2023\09\Data_732.BIN	2260	2285
12	E-W	30	2023\09\Data_732.BIN	2380	2405

The following figure provides an example of the recorded strain signal at Sensor 14 during the passage of the 12 calibration events during Day 1 (see Figure 8). Each of the main peaks in the signal corresponds to one calibration event. In addition to these primary peaks, smaller peaks are observed in the signal. These correspond to the passage of other vehicles that crossed the bridge between calibration events. This occurred because the calibration truck needed to drive to the nearest junction to change direction and cross the bridge again.

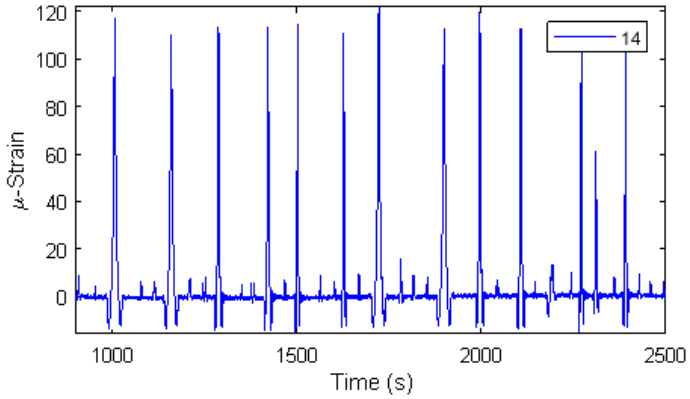

Figure 8: Full record of strain measured at Sensor 14 during the calibration runs on Day 1

Figure 9 shows the strain signals recorded during Event 1 of Day 1 for all strain sensors. These signals highlight discrepancies in measured values and underscore the need to apply a sensor-specific calibration factor. For instance, some sensors, such as 4 and 5, exhibit very high peaks, with strain values exceeding 200 μ-strain, whereas the sensor at mid-span (Sensor 14) barely registers values above 100. It is expected that the maximum strain during a vehicle crossing event should occur at the mid-span section. However, such discrepancies in strain magnitudes are typical and arise due to various factors, including the individual properties of each sensor, the quality and condition of the sensor's contact surface, the bond condition between the sensor and the carbon fibre plate, the adherence of the fibre plate to the concrete, and other local variabilities.

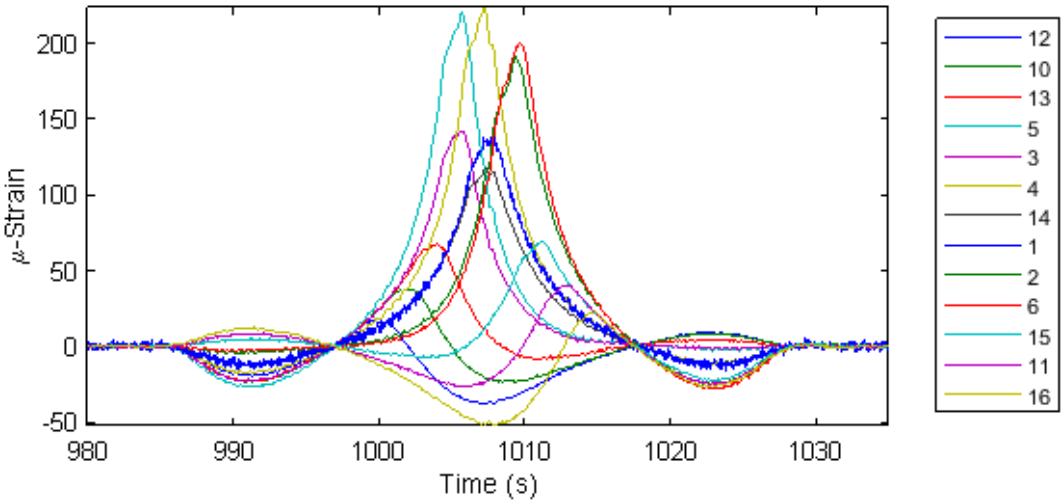

Figure 9: Signals for all strain sensors for Day 1 Event 1.

3.1.2. Calibration Day 2

The second calibration session was performed on 30th April 2024, using the 6-axle vehicle configuration shown in Figure 10. The tractor was a 3-axle Scania R164GA6X4NA truck towing a 3-axle trailer (0270 Damm DR4460) loaded with heavy machinery. During this test, the truck traversed the bridge at slow and constant speeds. Table 5 provides detailed information about the truck used during Calibration Day 2.

Table 5: Properties of Day 2 calibration truck

Axle number	Axle weigth (kN)	Axle spacing (m)	Axle distance (m)
1	86.0	-	0
2	80.4	3.500	3.500
3	80.4	1.355	4.855
4	72.0	5.320	10.175
5	72.0	1.810	11.985
6	72.0	1.810	13.795
Total	462.8	-	-

Figure 10: Day 2 calibration truck

Table 6 presents detailed information about each calibration event. The table includes information about the direction of travel, the filename containing the corresponding signals, and the approximate start and end times that delimit the event.

Table 6: Events for Day 2 calibration

Event number	Dir.	File name	Start time (s)	End time (s)
1	W-E	2024\04\Data_2018.BIN	1010	1070
2	E-W	2024\04\Data_2018.BIN	1485	1540
3	W-E	2024\04\Data_2018.BIN	1680	1730
4	E-W	2024\04\Data_2018.BIN	2165	2220
5	W-E	2024\04\Data_2018.BIN	2385	2438
6	E-W	2024\04\Data_2018.BIN	2910	2965
7	W-E	2024\04\Data_2018.BIN	3155	3205
8	E-W	2024\04\Data_2019.BIN	70	130

3.1.3. Calibration Day 3

The third calibration session was performed on 13th September 2024, using a 3-axle Scania R 560 truck loaded with gravel, depicted in Figure 11. During this test, the truck traversed the bridge at slow and constant speeds. Table 7 provides detailed information about the truck used during Calibration Day 3.

Table 7: Properties of Day 3 calibration truck

Axle number	Axle weigth (kN)	Axle spacing (m)	Axle distance (m)
1	89.1	-	0
2	85.0	3.300	3.300
3	85.0	1.350	4.650
Total	259.1	-	-

Figure 11: Day 3 calibration truck

Table 8 provides detailed information about each calibration event. The table includes information about the direction of travel the filename containing the corresponding signals, and the approximate start and end times that delimit the event.

Table 8: Events for Day 3 calibration

Event number	Dir.	File name	Start time (s)	End time (s)
1	E-W	2024\09\Data_301.BIN	2710	2770
2	W-E	2024\09\Data_301.BIN	2830	2880
3	E-W	2024\09\Data_301.BIN	3060	3120
4	W-E	2024\09\Data_301.BIN	3180	3230
5	E-W	2024\09\Data_301.BIN	3410	3470
6	W-E	2024\09\Data_301.BIN	3535	3585
7	E-W	2024\09\Data_302.BIN	235	280
8	W-E	2024\09\Data_302.BIN	345	395
9	E-W	2024\09\Data_302.BIN	605	655
10	W-E	2024\09\Data_302.BIN	725	770
11	E-W	2024\09\Data_302.BIN	965	1010
12	W-E	2024\09\Data_302.BIN	1080	1125

3.2. Speed estimation

Various techniques are available for estimating vehicle speed, as summarized in a recent review [7]. The following study compares three of these methods, utilizing signals from Channels 13 and 15. These channels were chosen to emphasize the limitations inherent in some of the existing approaches.

The simplest method for estimating speed involves calculating the time difference between signal peaks detected by sensors. By combining this time difference with the known distance between the sensors, an estimate of the vehicle's speed can be determined. However, this approach has notable drawbacks. It can yield inaccurate results if the peaks do not precisely correspond to specific vehicle axles or if the signals lack well-defined features for individual axles. Additionally, this method relies on a single point of data, making it highly susceptible to noise and dynamic effects, which can significantly distort the speed calculation.

A second, widely used method, described in [8], analyses the entire signal rather than relying solely on individual peaks. In setups using this technique, sensors are placed at locations designed to provide clear responses for each axle. The cross-correlation technique is then applied to the signals, using the time lag corresponding to the highest correlation to estimate the vehicle's travel time between sensors.

This method assumes that the two signals are similar in shape, with one being a shifted version of the other. However, this assumption often fails in practice, as demonstrated in [7] for simple bridge configurations, such as simply supported spans. The issue is also apparent in the case of the Herøysund Bridge, as shown in Figure 9. Here, the signals from Channels 13 and 15 (collected from sensors placed symmetrically 10 m from the mid-span) are mirrored rather than shifted. For example, Channel 13 shows a pronounced negative response before its maximum positive value, whereas Channel 15 exhibits the opposite pattern. This asymmetry causes the cross-correlation to be dominated by the large negative areas in the signals, complicating the identification of an accurate time lag for speed estimation.

To overcome these limitations, a novel theoretical approach called Convoluted Reciprocity (CR) was proposed in [7]. This method establishes a relationship between the convolutions of signals recorded at two locations for separate events. When the speed of one event is known, this relationship can be used to accurately determine the speed of the other event. Unlike traditional methods, CR uses information from the entire signal and does not depend on the signals having a specific shape or being shifted versions of one another. This approach has been derived theoretically, tested through numerical simulations, and validated experimentally. Consequently, CR is used as the reference solution in the present analysis.

To assess the performance of these speed estimation methods, all 32 calibration events conducted over three days were analysed. Figure 12(a) presents the speed estimation results for these events. With the Convoluted Reciprocity method serving as the benchmark, Figure 12(b) displays the errors associated with the alternative techniques. The cross-correlation method consistently underestimated the speed by approximately 10%. The peak-based method exhibited variable accuracy, depending on the vehicle configuration. For instance, it produced relatively accurate results for the 3-axle trucks used on Days 1 and 3, with errors fluctuating around zero. However, for the 6-axle vehicle used on Day 2, the method consistently underestimated speed, highlighting its sensitivity to the vehicle's axle configuration.

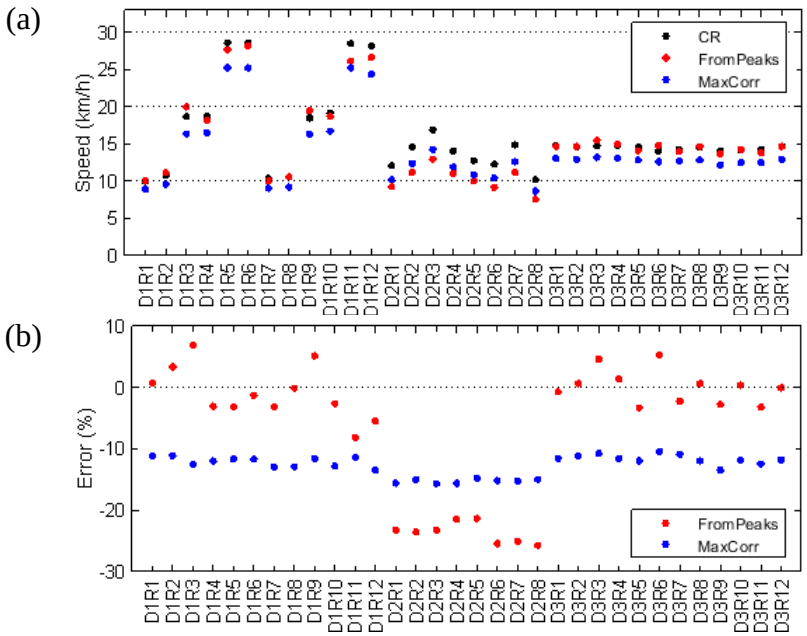

Figure 12: (a) Speed estimates of calibration events for different methods; (b) Speed estimate errors taking CR method as reference.

3.3. Influence line calculation

For the calibration events, we possess all the necessary data to derive the influence lines (IL) at all sensor locations. To obtain the ILs we require the recorded bridge signals and detailed information about the vehicle loading, such as the vehicle's speed, axle configuration (number and spacing), and the load on each axle. Using this information, the influence line can be determined by solving the inverse problem through a method commonly referred to as the matrix method [9]. This approach employs a least-squares fit to calculate the coordinates of the IL. However, due to the numerous unknowns to be solved, the solution lacks robustness. To improve reliability, it is customary to analyse multiple vehicle passages and compute an average influence line. Further discussions on influence line extraction techniques and alternative methods are available in [10].

In this study, additional conditions were imposed to enhance the accuracy of influence line (IL) extraction. For instance, the algorithm was refined by constraining the IL to approach zero near the column locations. Additionally, the extracted vehicle speed was fine-tuned to minimize the reconstruction error. Due to partial system failures after June 2024, which significantly reduced the number of functional sensors during Calibration Day 3, the IL extraction was carried out only for Calibration Days 1 and 2. The resulting ILs, presented in Figure 13, are obtain for a unit load of 1 kN instead of 1 N.

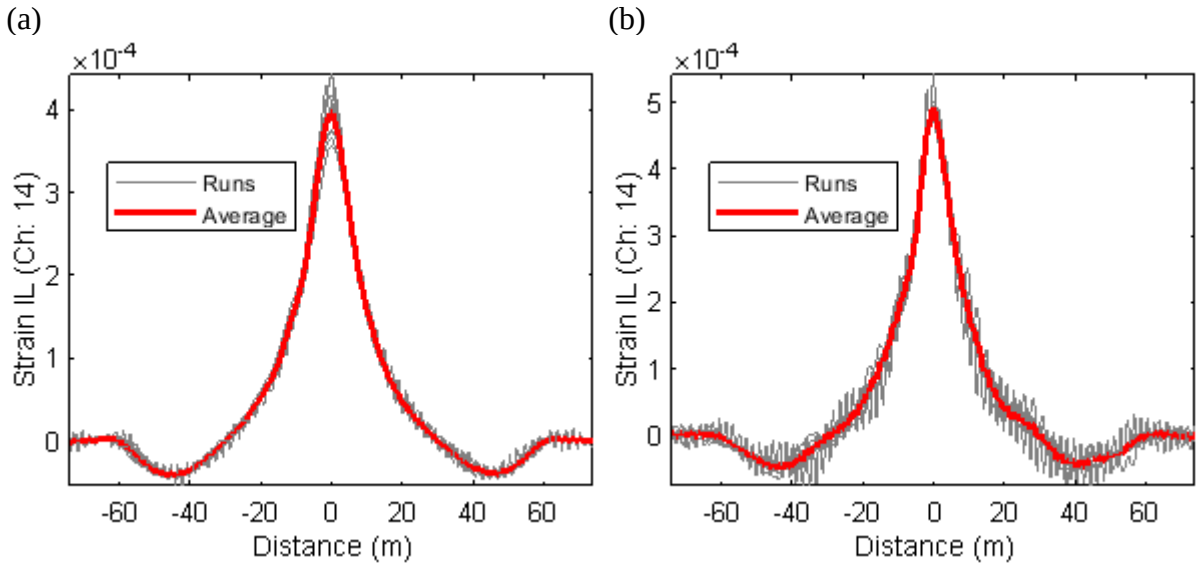

Figure 13: Influence lines for Sensor 14; (a) Calibration Day 1; (b) Calibration Day 2

The influence lines derived from the calibration events show notable differences between the results of Day 1 and Day 2. Specifically, the magnitude of the influence line is larger for Day 2, and its shape exhibits greater variability across the runs. This increased variability may stem from larger uncertainties in the vehicle configuration data, particularly due to factors such as the vehicle's length and the number of axles. To further investigate these discrepancies, the average daily influence lines were compared at four selected sensors, illustrated in Figure 14, providing a clearer picture of the observed differences.

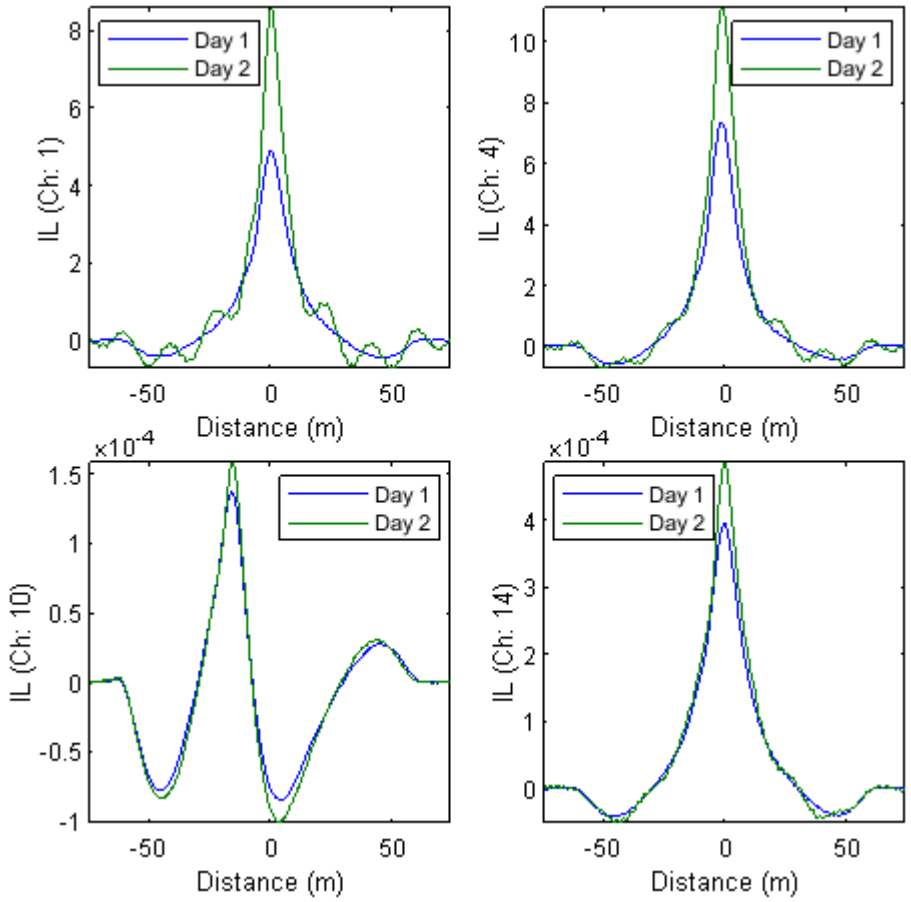

Figure 14: Comparison of daily average influence lines for a selection of channels

Initially, the differences in the magnitude of the influence lines were attributed to potential issues in the extraction procedure. Due to the bridge's considerable length, the mathematical process for deriving the influence line is not particularly well-conditioned, making it sensitive to minor discrepancies in measurements or calibration truck data. However, as will be discussed later, a more plausible explanation lies in the non-linear behaviour of the structure. This hypothesis aligns with the influence line results shown in Figure 14, where the heavier vehicle used on Day 2 produces influence lines with greater magnitudes.

For completeness, Figure 15 illustrates the extracted influence lines at all sensor locations, derived from the average results of the Day 1 calibration. Using this method, it is possible to successfully obtain the influence lines for every sensor position.

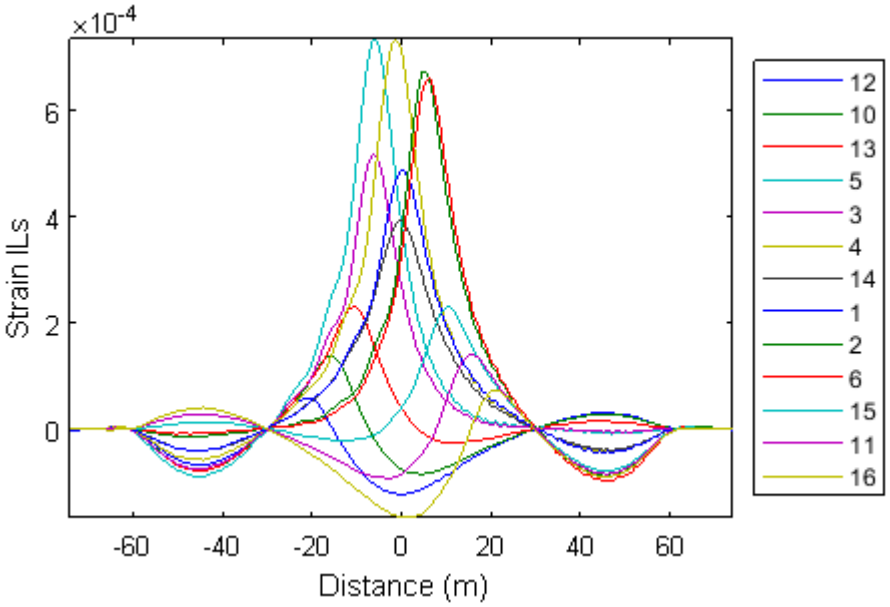

Figure 15: All influence lines for extracted from calibration Day 1

3.4. GVW calculation and calibration factors

The Gross Vehicle Weight (GVW) of a vehicle is directly proportional to the area under the measured signal recorded during its crossing, a technique often referred to as the "area method." This method is well-documented in the literature (e.g., [11] and [12]). The fundamental principle is given in Eq. (3), where the signal *S* is integrated over the spatial domain. To convert the signal from the time domain to the spatial domain, the vehicle's speed must be determined. The calibration factor is calculated as the ratio of the GVW to the signal area and requires the known weight of a reference vehicle. Once determined, this factor can be used to estimate the GVW of vehicles with unknown weights.

$$GVW = (GVW\ Factor) \cdot \int S(x)dx \qquad \text{Eq. (3)}$$

Results for a specific sensor (Channel 6) are shown in Figure 16, which presents the GVW factors for all calibration runs, grouped by calibration days. The sensor factor is computed for each calibration event, revealing some variation within events on the same day. These minor fluctuations in the factors are attributed to noise and dynamic effects. However, more significantly, the results indicate a distinct difference in the sensor factor between days, with notably smaller values observed on Day 2. This required further investigation to identify the underlying cause.

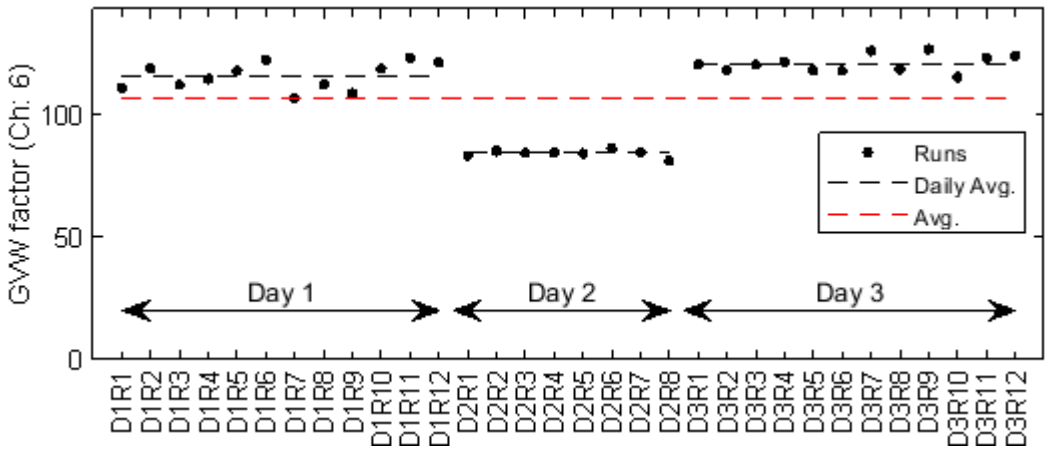

Figure 16: GVW factors for each calibration Day and Run

At first, it was hypothesized that temperature could be causing the observed variations. To explore this, the factors obtained for each calibration event were plotted against the average temperature recorded during each event, as shown in Figure 17. However, the temperatures across the three calibration days were rather similar, and no clear correlation was observed. Although the largest temperature difference occurred between Day 1 and Day 3, their GVW factors were similar. In contrast, Days 1 and 2 had more similar temperatures, yet their GVW factors differed significantly. This analysis suggested that the variations in the results could not be solely attributed to the effect of temperature on the bridge.

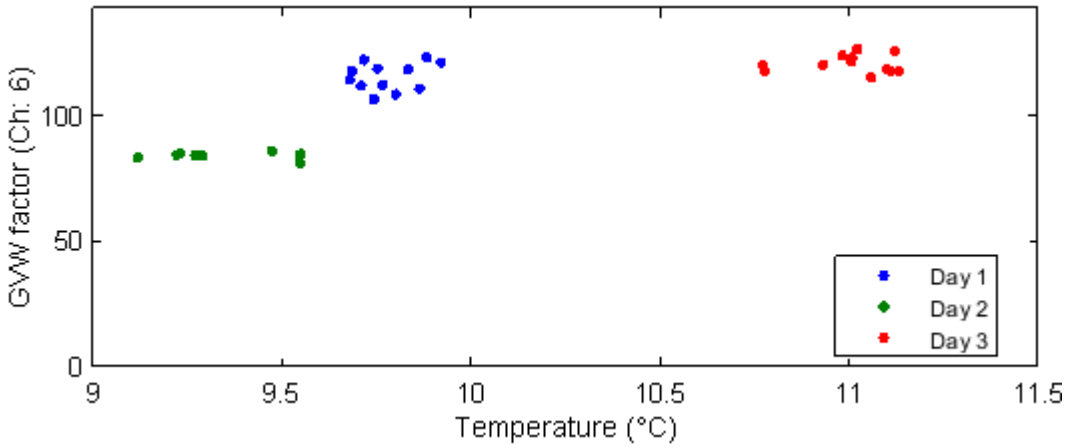

Figure 17: GVW factors with respect to the event's recorded temperature.

It is thought that the change in magnitude is linked to the inherent non-linear behaviour of the structure. As a cracked prestressed bridge, the structure theoretically exhibits a non-linear moment-curvature relationship, where the location of the neutral axis depends on the applied moment (vehicle load) and the axial force (prestressing). More details on this can be found in [13]. In addition, other factors contributing to non-linearity, such as material or geometric properties, may also play a role. The moment exerted by the calibration vehicle on Day 2 is significantly larger than that on the other calibration days, as indicated in Table 2. Heavier vehicles produce a greater response from the bridge, leading to smaller GVW factors.

The non-linear relationship is not the same for all sensors. When the same analysis is repeated across all sensors, they show a different dependency on the load. Figure 18(a) illustrates that the ratio of factors between Day 2 and Day 1 is consistently below 1, indicating that the Day 2 factors are smaller than those on Day 1 for all sensors. Since Day 2 corresponds to the heavier

vehicle, this suggests the presence of non-linear behaviour. In contrast, Figure 18(b) shows the ratio of Day 3 to Day 1, with results oscillating around 1, indicating that the factors for these two days are similar. However, no clear spatial trend can be observed in any of these results, as the factors do not correlate clearly with the sensor locations.

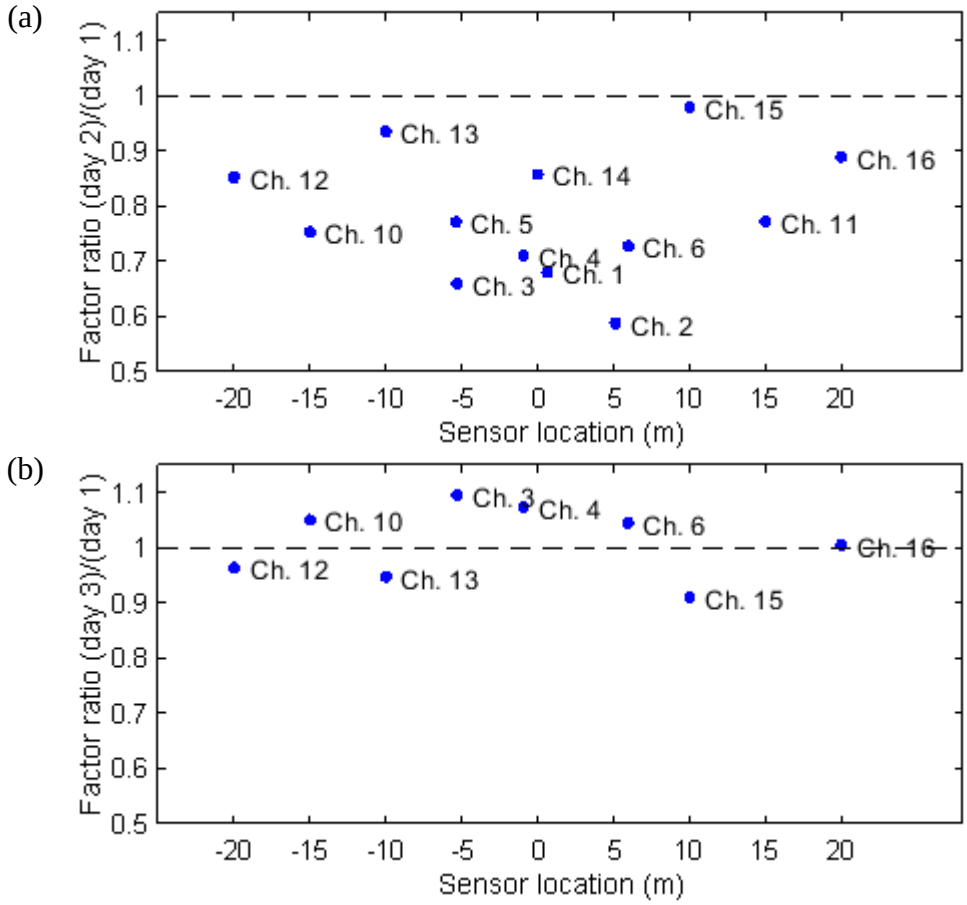

Figure 18: GVW factor relations for different sensors;
(a) Day 2 to Day 1 ratio; (b) Day 3 to Day 1 ratio.

4. Master thesis works

The development of a Structural Health Monitoring (SHM) system for detecting damage in post-tension systems was proposed as a potential topic for master thesis work to students at NTNU. Following initial discussions with their supervisor, the students explored possible directions for their research. Ultimately, the final topic was tailored to align with the students' interests and was mutually agreed upon in collaboration with their supervisor.

Considering this context, three master theses were developed during the project's duration. These included:

- Thesis 1 – Title: "*Model validation with measurements and effect of damage on strain signals*" (WP1.A3.NTNU.Thesis1) [14]
- Thesis 2 – Title: "*Quantifying Structural Damage on the Herøysund Bridge through Strain and Displacement Response Analysis*" (WP1.A3.NTNU.Thesis2) [16]
- Thesis 3 – Title: "*Machine learning-assisted structural health monitoring of Herøysund Bridge*" (WP1.A3.NTNU.Thesis2) [17]

The following subsections provides a detailed summary of each thesis separately. These summaries outline the objectives, methodologies, and key findings of each study, highlighting their contributions to the overarching goal of developing a Structural Health Monitoring (SHM) system for post-tension systems.

4.1. Influence line calculation (WP1.A3.NTNU.Thesis1)

The work presented in this section corresponds to the master thesis [14], designated under the codename WP1.A3.NTNU.Thesis1. Table 9 provides a summary of the bibliographical details for this document, outlining essential information for reference.

Table 9: Bibliographical information for WP1.A3.NTNU.Thesis1

Title:	Model validation with measurements and effect of damage on strain signals
Author(s):	Sindre Moritsgård Flatjord
Date:	June 2023
Language:	English
Codename:	WP1.A3.NTNU.Thesis1
Link:	https://ntnuopen.ntnu.no/ntnu-xmlui/handle/11250/3093185

This master thesis initiated a numerical investigation to assess the feasibility of detecting damage in post-tensioned systems through continuously monitored strain measurements. A 3D model was developed in DIANA, with the model's geometry and prestressing parameters processed programmatically. The model was validated against the 50-tonne test reported in [15]. Various damage scenarios were simulated to analyse their impact. The study specifically focused on evaluating the effects of damage on the static response of the bridge under its self-weight and the quasi-static response under the influence of a passing vehicle.

To achieve this, the work focused on determining the influence lines, which were generated using DIANA's movable load tool. A highly detailed 3D model of the bridge was developed, incorporating the exact geometry of all structural details and the tendons' layout (see Figure 19).

(a)

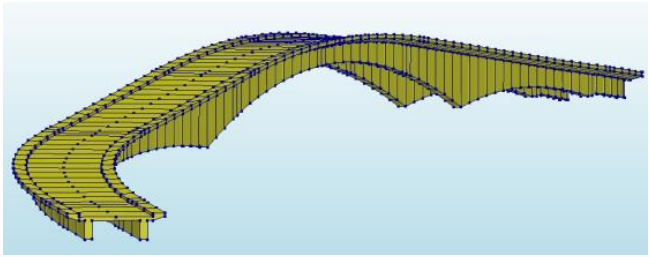

(b)

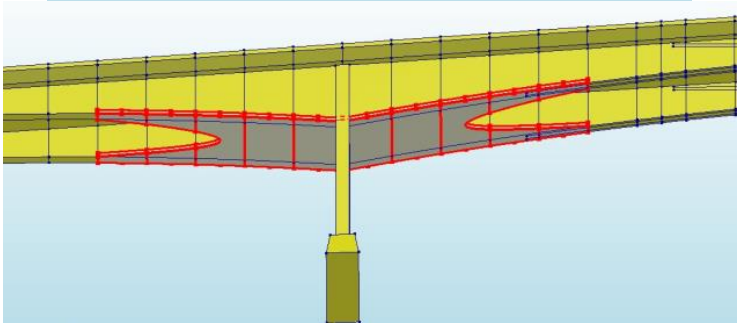

Figure 19: (a) Overview of 3D numerical model of Herøysund Bridge;
(b) Detail of the geometry near the columns. (Source: [14])

The numerical model was validated against the measurements obtained from the 50-tonne test reported in [15]. Validation was carried out by comparing the model's results with observed data, specifically focusing on the vertical displacement at the mid-span and the strain values induced by the vehicle load alone. The validation load case is shown in Figure 20.

(a)

(b)

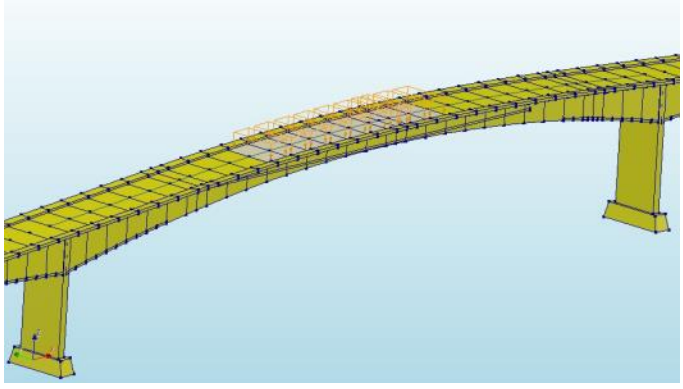

Figure 20: (a) 50 tonne vehicle on the bridge;
(b) Numerical model with the load of the vehicle (Source: [14])

To detect post-tension damage from the strain signal, the study investigates two components. The first component is the static load due to the bridge's self-weight, representing the unloaded bridge state. While the bridge is continuously monitored, the strain values recorded when the bridge is not subjected to traffic loads should remain constant. However, if the post-tension system experiences a sudden tendon failure, it is expected that the strain values will exhibit a noticeable jump, as illustrated in Figure 21. This phenomenon is referred to in this work as the "Static Strain."

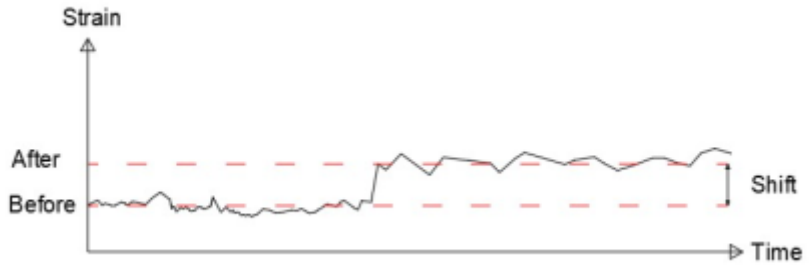

Figure 21: Schematic description of expected strain value shift due to tendon breakage (Source: [14])

The magnitude of the change in static strain depends on the number of broken tendons and the extent of the tendon damage. The study explores several different damage scenarios to assess this relationship. It was found that the effect of localized tendon breakage with a small extent was minimal. Nevertheless, greater strain shifts were observed in the sensors located closest to the damage. Conversely, if the damage affected the entire tendon, the strain shift was more uniformly distributed across the sensors.

On the other hand, the study also explores the variation in strain responses under vehicle passage, referred to as the "quasi-static" strain. To achieve this, the mobile load tool from DIANA was essential, as it allows for the generation of influence lines at the desired sensor locations. The tool, along with the impact of damage on the influence lines, was initially tested on a beam model, as shown in Figure 22. The model consists of a simply supported beam with a continuous prestressing system featuring a constant eccentricity. Prestressing steel was then progressively removed, either partially or entirely. The strain responses at location A, situated in the middle of the left span, were investigated numerically.

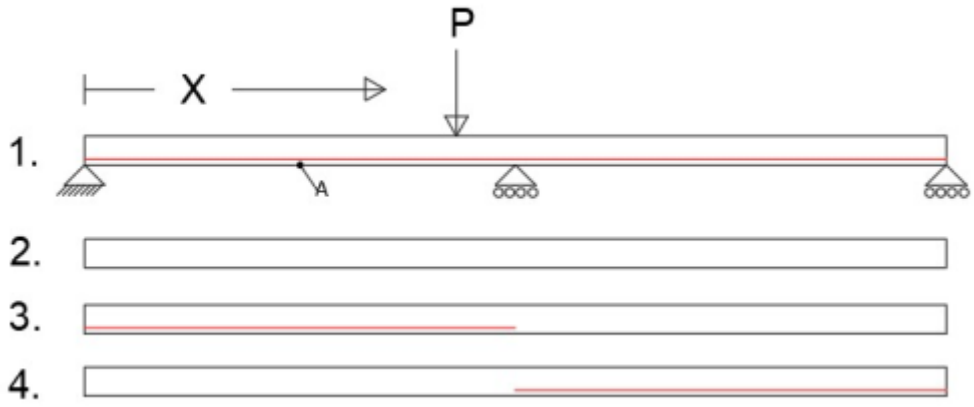

Figure 22: Damage cases in the test model (Source: [14])

The variations in cross-sectional stiffness across the beam influence the magnitude of the influence lines, as shown in Figure 23. When the missing tendon is located on the opposite span of the measurement point (as seen in Case 3 compared to Case 1), there is no significant difference in strain. However, when the steel is absent on the same span as the measurement point (Cases 2 and 4), the change in strain becomes more pronounced. From this numerical example, it can be concluded that the strain responses under passing vehicles are indeed affected by damage to the post-tension system. The magnitude of the strain change will depend on both the location and extent of the damage.

(a) (b)

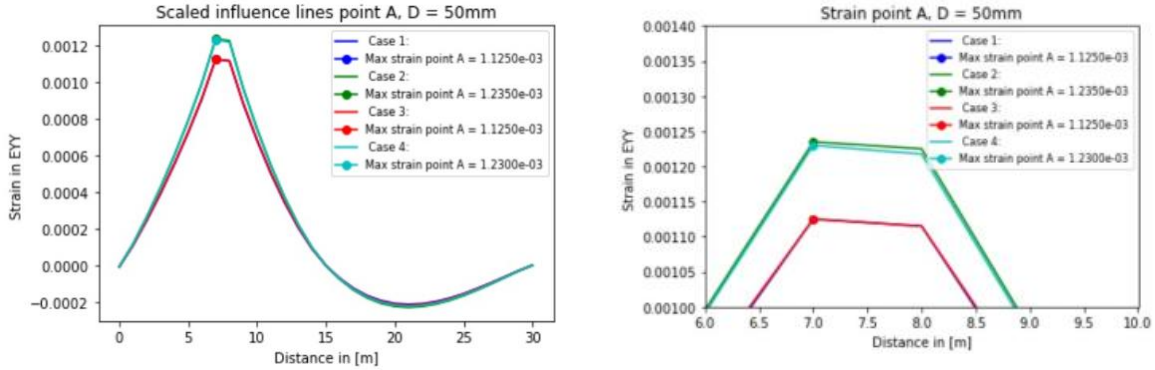

Figure 23: (a) Strain influence lines for different damage cases;
(b) Zoom in on the maximum values (Source: [14])

To quantify the effect of damage on the Herøysund Bridge, this study utilised the validated numerical model to explore various damage locations and extents. The influence lines at several sensor locations were then calculated. However, due to the complex geometry of the bridge, the obtained influence lines exhibited some numerical issues. Figure 24 illustrates the numerical influence lines, which display a noticeable jump at around 33 metres. Despite extensive efforts, this numerical problem could not be resolved. One potential cause was identified in the vertical variation of the road (the varying elevation of the deck), which likely affected the performance of the mobile load tool.

Nevertheless, the study continued to investigate the effect of damage on the quasi-static component. The trends observed were similar to those for the static component, with larger variations seen in sensors located near the damage. However, the magnitude of the strain change was generally smaller in the quasi-static component compared to the static component.

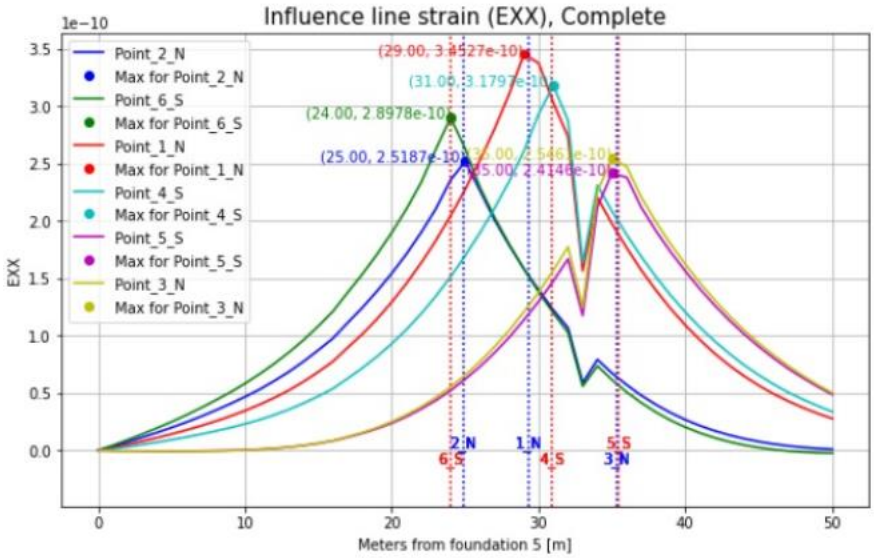

Figure 24: Influence lines for several sensor locations of the Herøysund Bridge. The results feature a sudden jump due to a numerical error that could not be fixed on time. (Source: [14])

Despite the numerical errors in the results and the limited number of case studies, this work has laid the foundation for the subsequent master thesis. It addressed and resolved several issues related to DIANA modelling, particularly when using the mobile load tool. Additionally, the work provided copies of the Python framework used to generate the numerical model of the bridge and to conduct the numerical analysis, offering valuable resources for the following master thesis.

The study found that the largest strain deviation occurred when two prestressed cables were removed, causing an 8% increase in strain, equivalent to 27 µm/m. In comparison, daily temperature fluctuations can cause strain changes up to 100 µm/m. When using the mobile load, the greatest variation in strain compared to an intact bridge was about 4.5%, or 15 µm/m. The response of strain sensors to different defects varied: small damage to the post-tensioned steel primarily affected sensors close to the defect, with strain increases in nearby sensors and decreases in others. If an entire post-tensioned cable was removed, the strain change became more uniform across sensors, especially within the affected beam.

The study suggests that damage location can be inferred by analysing the strain patterns across sensors. If all sensors on one side show increased strain, it may indicate damage to an entire tendon in the beam. Conversely, if some sensors show increased strain and others decreased, it may suggest localized damage. These results highlight the potential of strain measurements for detecting and localizing damage, though the changes observed were relatively small compared to temperature-induced variations.

4.2. Effect of damage (WP1.A3.NTNU.Thesis2)

The work presented in this section corresponds to the master thesis [16], designated under the codename WP1.A3.NTNU.Thesis2. Table 10 provides a summary of the bibliographical details for this document, outlining essential information for reference.

Table 10: Bibliographical information for WP1.A3.NTNU.Thesis2

Title:	Quantifying structural damage on the Herøysund Bridge through strain and displacement response analysis
Author(s):	Nora Svae Eggum, Margrete Furnes
Date:	June 2024
Language:	English
Codename:	WP1.A3.NTNU.Thesis2
Link:	https://ntnuopen.ntnu.no/ntnu-xmlui/handle/11250/3153539

The objectives of this study include creating a simplified model of the Herøysund Bridge, developing Python scripts to facilitate parametric studies, and quantifying the magnitude of response variations at different locations across the bridge. Linear analyses were conducted in DIANA to examine prestress damages. Prior to these analyses, the Herøysund Bridge model was validated, confirming the appropriateness of the meshing and revealing that the modelled passive reinforcement had minimal impact on the results. Given its negligible effect on the outcome but significant influence on analysis runtime, the passive reinforcement was removed.

A literature review was conducted to explore existing work in damage detection, providing an overview of the field and identifying this study's contribution. The review found that most studies in this area have focused on simple beams with multiple spans and constant cross-sections. In contrast, this investigation, despite some simplifications, focuses on a real bridge, offering valuable contributions to the field. The goal of this thesis is to build on the work presented in [14], improving and extending it. For this, a simplified numerical model of the bridge was developed, revised Python scripts were created, and numerical investigations were carried out for an extended number of damage scenarios, with a focus on variations in strain and vertical displacements in both the static and quasi-static components.

It is acknowledged that the measured components are influenced by operational conditions, with temperature being the most significant contributing factor. To provide an indication of the variations in the measured strain, Table 11 presents the approximate order of magnitude of the strain values for different types of vehicles and temperature conditions.

Table 11: Approximate strain fluctuations due to different loads (Source: [16])

Type of loading	Strain fluctuation $[\mu m/m]$
Heavy trucks	250
Normal vehicles	20
Temperature variation	75 (max variation)

This work examines the effect of damage on two components: the change in static response and the change in vehicle response. These effects are conceptually illustrated in Figure 25, which shows the expected variations in strain due to tendon breakage.

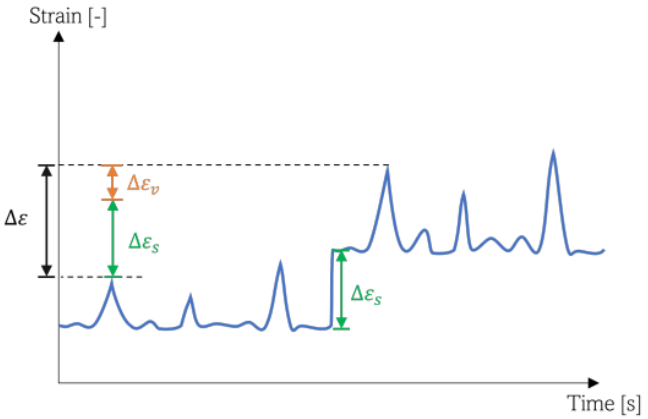

Figure 25: Strain values over time following a tendon breakage (Source: [16])

The magnitude of the variations in both the static and vehicle components is evaluated using the numerical model of the Herøysund Bridge (see Figure 26). Compared to previous work, the bridge has been simplified by assuming a constant elevation of the road surface. Additionally, some construction details are simplified, and the structure is considered symmetric. The effect of ordinary reinforcement is also assessed, with the conclusion that it is appropriate to exclude it from the parametric study of different damage scenarios. With these considerations, the study adopts a simpler yet sufficiently accurate description of the bridge, allowing for efficient and repeated simulations.

(a)

(b)

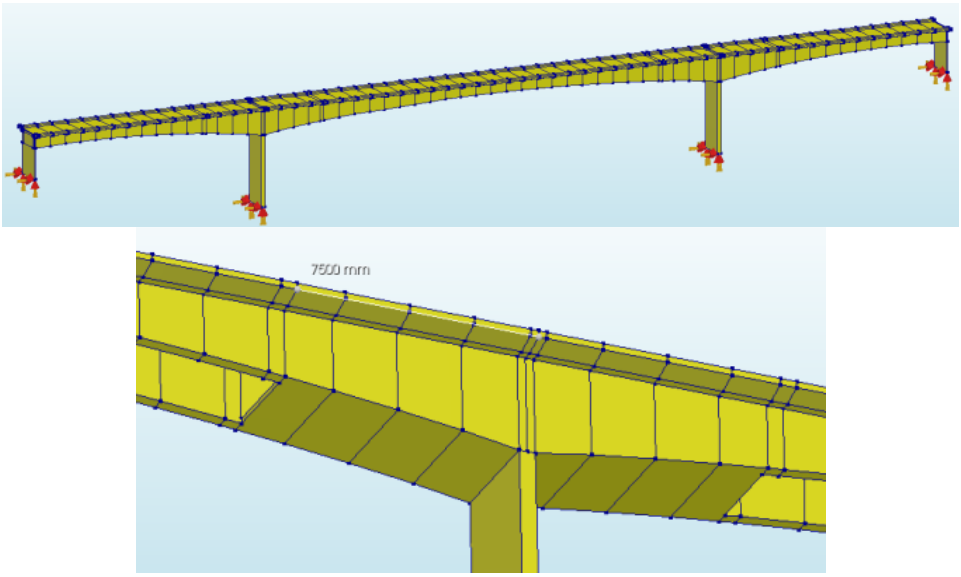

Figure 26: (a) Global view of numerical model of the Herøysund Bridge;
(b) Simplified modelling of the detail near the columns (Source: [16])

A broken post-tension tendon is modelled as a discontinuity in the active steel of the bridge, centred around the location of the tendon breakage. The length of this discontinuity depends on the size of the void at the breakage location and the transmission length. In reality, the prestressing force on the structure increases from zero to its maximum value along the transmission length. However, this process is simplified in this study, as illustrated in Figure 27, where the effective prestressing force on the structure is schematically represented.

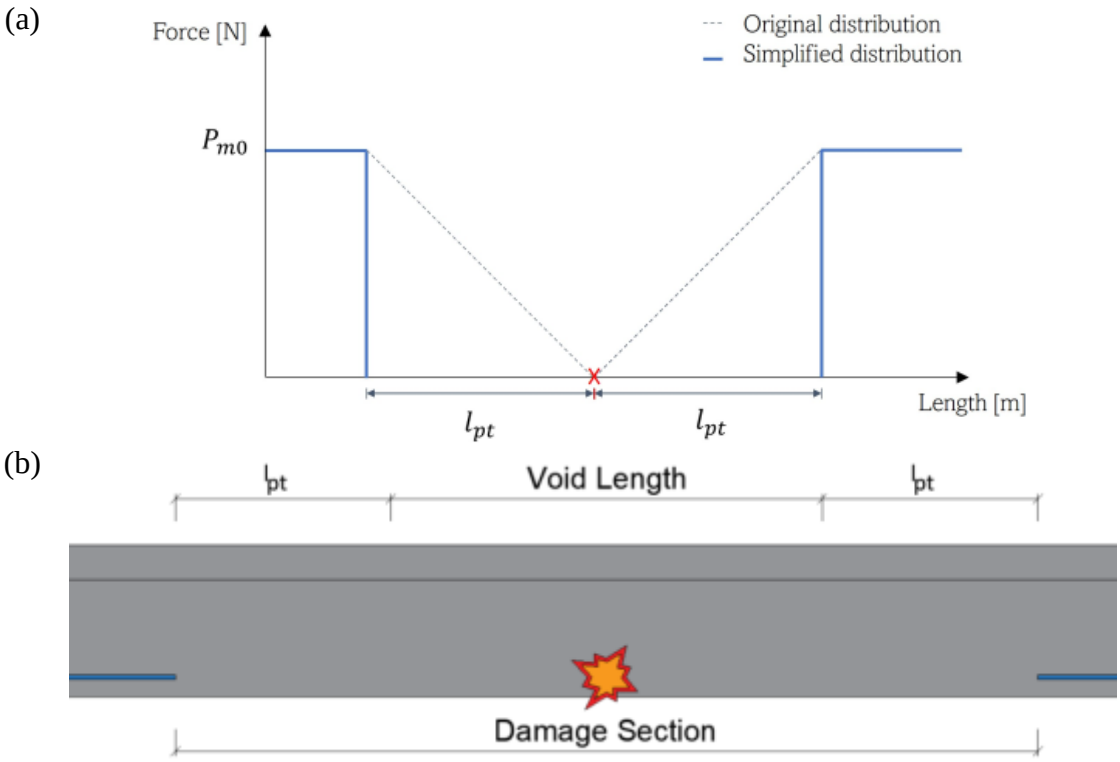

Figure 27: Schematic description of prestressing force at the vicinity of a tendon breakage; (a) Prestressing force; (b) Extent of damage including void length (Source: [16])

This study evaluates the changes in responses due to damage at four specific sensors. The sensor locations correspond to four of the sensors from the real instrumentation system installed on the Herøysund Bridge. The equivalency between the sensor numbering used in this work and the actual channel numbering is provided in Table 12, with a coordinate system centred at the mid-span. The particular sensors considered in this study are also listed in Table 12.

Table 12: Location of strain gauges

Sensor Number	Channel number	Beam (North / South)	x-value in system (mm)	x-value in [16] (mm)
7	16	South	20 000	40 000
8	15	South	10 000	50 000
9	14	South	0	60 000
12	11	North	15 000	45 000

First, the study examines the variation due to the vehicle component (quasi-static). This is evaluated by analysing the changes in the influence line. Figure 28 illustrates the influence line of strain at mid-span for both the healthy and damaged bridge. The same plot also shows the difference between the two, with the vertical scale indicated on the right y-axis. The grey shaded area highlights the location and extent of the damage in the prestressing system.

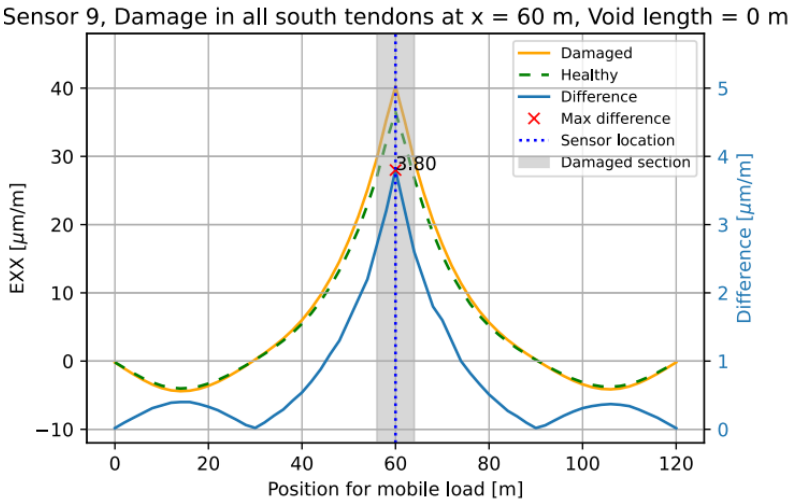

Figure 28: Strain influence lines and their difference for healthy and damage bridge (Source: [16])

The same study is repeated for various damage locations and lengths of the voids. However, it is difficult to generalise the results, as different sensor locations exhibit varying sensitivities to damage. Additionally, the extent of the damage has a distinct impact on each location. The influence lines change in both shape and magnitude depending on the damage. To systematically compare different damage scenarios, the changes in influence lines are evaluated using the R^2 value. The results of the extended parametric study are summarised in Figure 29. In general, larger differences (smaller R^2 values) are observed for damage closer to the mid-span section (60 m), though this trend is not uniform across all studied sensor locations.

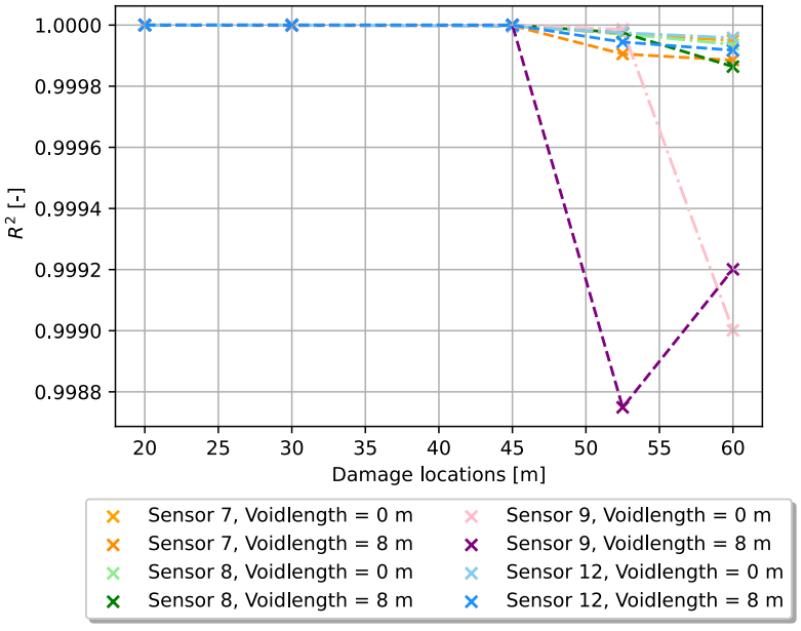

Figure 29: R^2 values for various sensor locations, damage locations and void length. (Source: [16])

The study is extended to consider the scenario where a damaged tendon is equivalent to the loss of prestress force and reinforcing steel along its full length. In this case, the influence of removing multiple tendons is evaluated. An overall trend of a reduction in R^2 values is observed

(Figure 30) for cases where more tendons are removed; however, these trends vary for each sensor. As expected, Sensor 9 (at mid-span) exhibits the greatest sensitivity to damage.

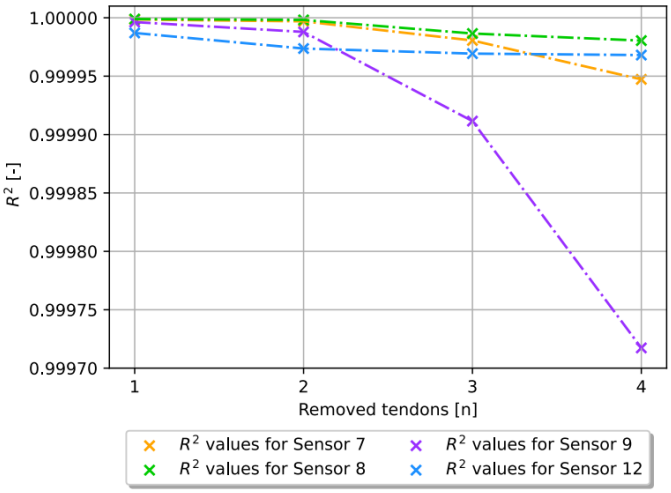

Figure 30: R^2 values when removing entire tendons (Source: [16])

Another effect of damage evaluated in this study is its impact on the static component of strain. For instance, the strain value of Sensor 9 under static load (self-weight) is shown with the dashed line in Figure 31, reporting a value of approximately -20 µ-strain. The study is then repeated for a damaged bridge with a void length of 8 m and various damage locations. Each damage scenario results in a new strain value under static load. However, the key quantity is the change in strain between the healthy and damaged cases, which is indicated by the blue line and blue values. It can be observed that when the damage is located far from the sensor, the sensitivity to damage is significantly reduced.

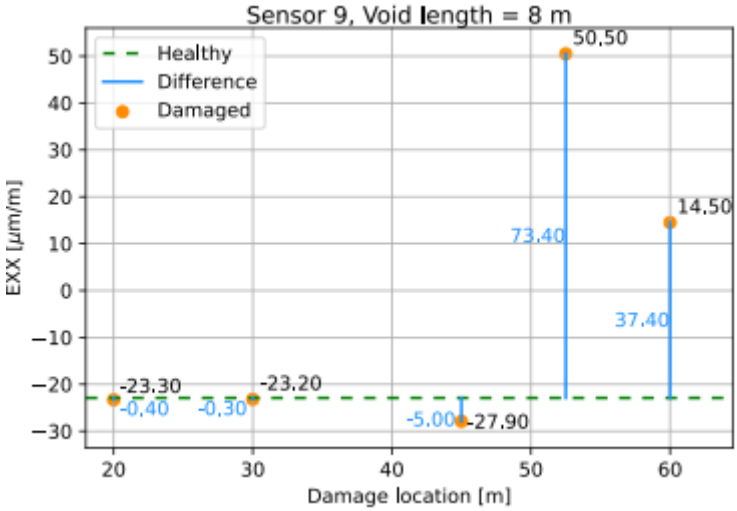

Figure 31: Static strain differences at Sensor 9 for a damaged tendon with 8 m void length at various damage locations (Source: [16])

Furthermore, the sensitivity to damage varies for each sensor. This is evaluated and summarised in Figure 32, which shows the difference in strain values due to damage. While it can generally be concluded that the maximum difference is observed when the damage is near the sensor, the trends and magnitudes of these changes differ significantly across the sensors.

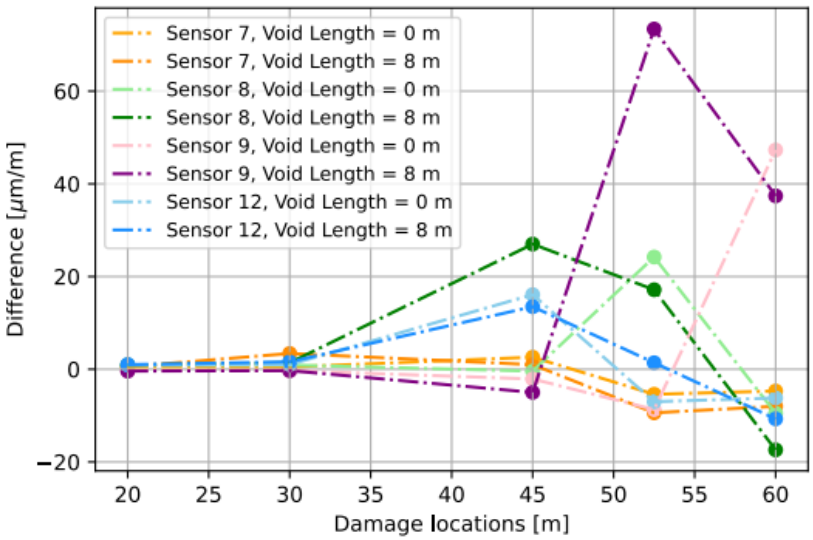

Figure 32: Static strain differences for all sensors and various damage scenarios (Source: [16])

However, if the damage corresponds to the complete removal of tendons, the damage is more severe, and in this case, the trends are clearer (Figure 33). Sensor 9 (at mid-span) shows the greatest sensitivity to this type of damage.

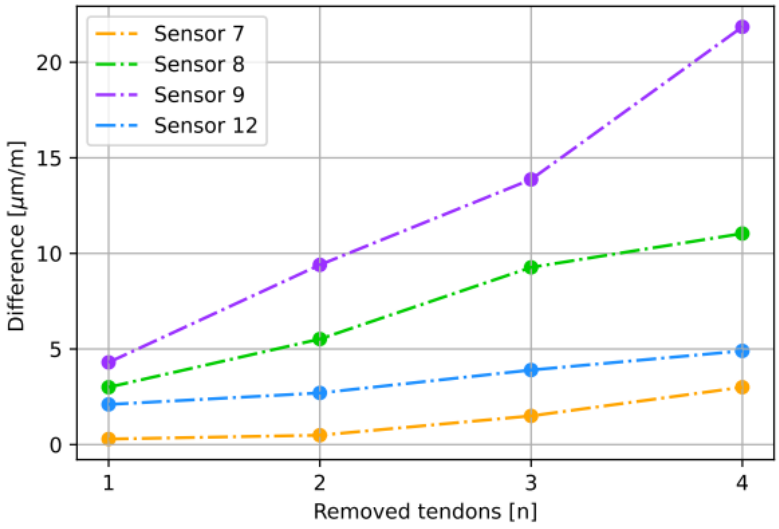

Figure 33: Static strain differences when removing entire tendons (Source: [16])

This study extends the analysis to consider another load effect, where, instead of measuring longitudinal strain, vertical displacement is recorded at each sensor location. By focusing on vertical displacement, the work aims to assess how the damage affects the structural response in terms of deflection rather than strain. This approach provides a broader understanding of the structural integrity, as vertical displacement can reveal different sensitivities to damage compared to strain measurements. The analysis is repeated for each sensor location, allowing for a comprehensive evaluation of the impact of tendon damage on the bridge's deflection behaviour under different damage scenarios.

The figures below illustrate the sensitivity of vertical displacement to various damage scenarios. Similar to the strain analysis, the study is divided into two local damages (Figure 34(a)) and entire tendon damages (Figure 34(b)).

(a)

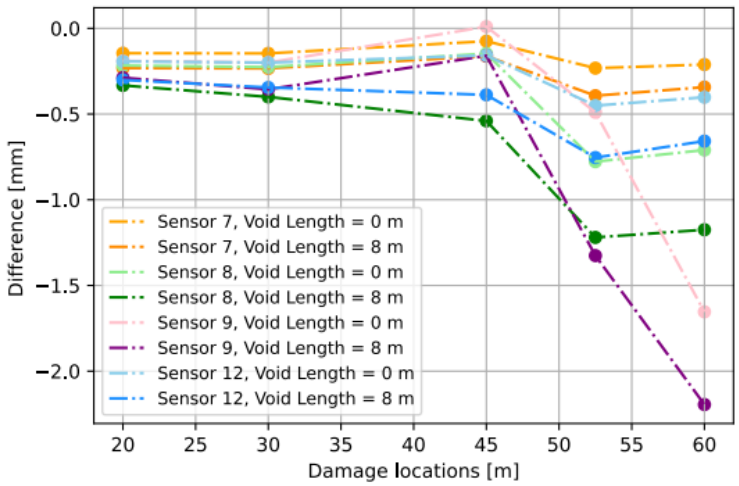

(b)

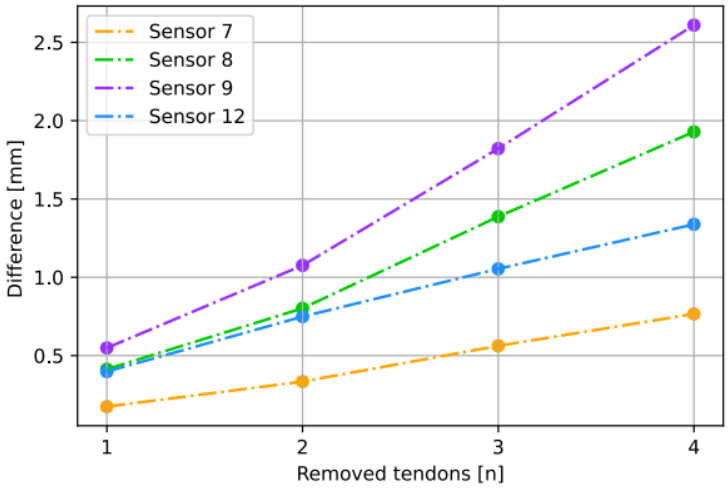

Figure 34: Difference in vertical displacement for:
(a) local damage; (b) full tendon removal (Source: [16])

To summarise the results, the work compares the effects of both damage effects (static and quasi-static) for both load effects (strain and displacement). For the specific case of Sensor 9 (at mid-span), with damage at the same location and a void length of 8 m, the response over time is examined for the passage of the same vehicle, both before and after the damage. This is shown in Figure 35. The results indicate that for strain signals, the static effect (37.4 μ-strain) is 10 times greater than the quasi-static effect (3.6 μ-strain). The difference is even more pronounced for displacements, where the static value (2.195 mm) is over 20 times greater than the quasi-static value (0.095 mm). From this example, it is also evident that the effect of damage on the influence line is greater for strain. In relative terms, the maximum change in the strain influence line is 8.9%, compared to just 1.8% for the vertical displacement influence line.

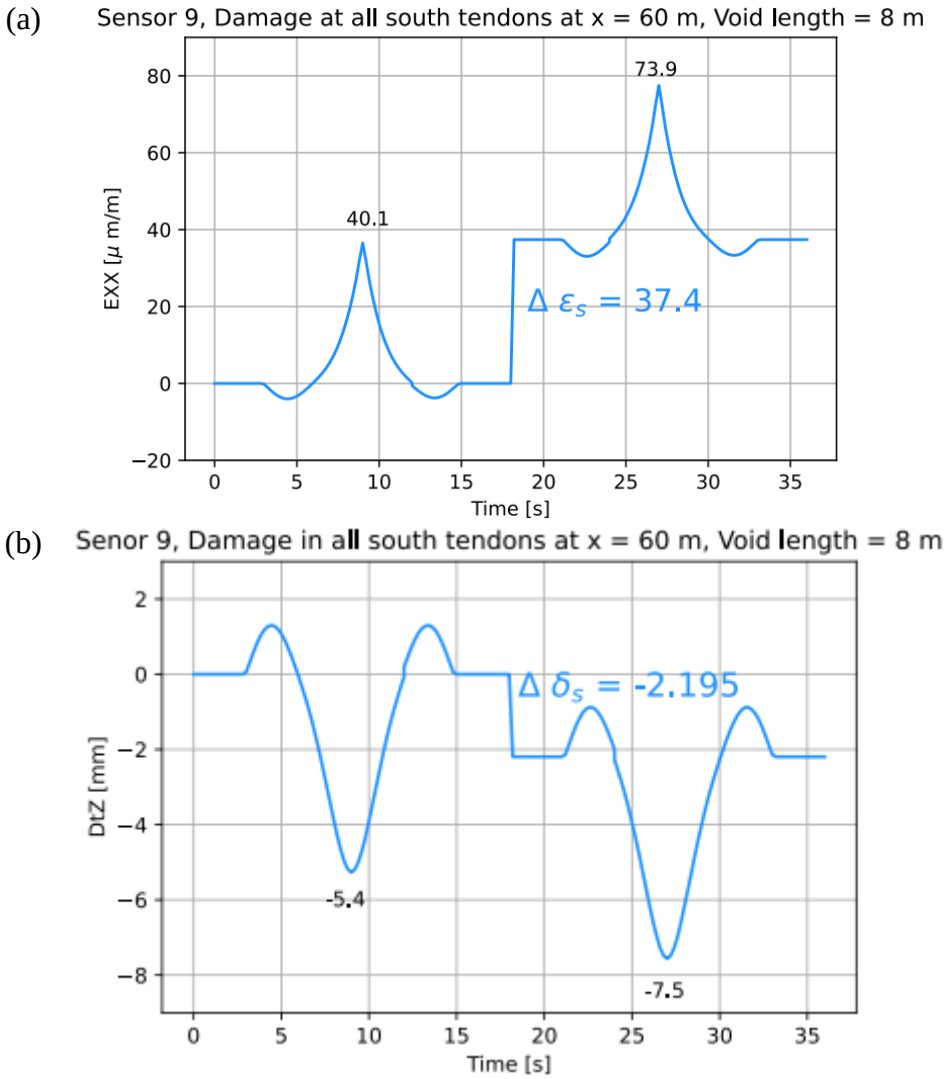

Figure 35: Time history of a vehicle passage before and after broken post-tension system with a 8 m long void; (a) Strain response at mid-span; (b) Vertical displacement at mid-span (Source: [16])

This work concludes that the findings from the parametric studies reveal that the stiffness of the cross-section at both the sensor and damage locations significantly affects the magnitudes of the responses. Furthermore, the results indicate that variations in strain responses are closely associated with local curvature changes, with more severe damage leading to more pronounced differences in displacement. While changes in influence lines across different damage scenarios showed only minor differences. In contrast, investigations into the response changes under static loads revealed significantly larger differences. Ultimately, the study concludes that while changes in responses due to damage can be detected in sensor measurements, they generally require substantial damage to be noticeable.

It was found that changes in strain responses were highest at the ends of a damaged section due to the greatest changes in curvature in these areas. The study also revealed that sensors are most responsive when the damage occurs in the same beam. The impact of void length was emphasised, as more extensive damage significantly amplifies differences in displacement responses. Additionally, as the void length increases, the difference in strain responses tends to decrease, especially when sensors are placed very close to the damage location.

Furthermore, comparison plots from the parametric studies consistently showed that removing entire tendons leads to more uniform response changes compared to localized damage scenarios. In general, the results demonstrated greater sensitivity of strain to damage conditions compared to vertical displacement. Regarding the two contributions, variations in load effects due to the quasi-static component were an order of magnitude smaller than those from the static component. Although the magnitude of the reported variations is small, they are likely to be overshadowed by operational variations in load effects, particularly those stemming from ambient temperature changes.

This work confirms that damage produces detectable changes in sensor responses, but it cannot definitively confirm if these changes would be detectable under normal operational conditions. It suggests that further research is necessary to better understand these effects, and provides a Python framework for creating models in DIANA, adding both passive and active reinforcement, including potential damage, performing mobile load analysis, and conducting static analyses.

4.3. Temperature compensation (WP1.A3.NTNU.Thesis3)

The work presented in this section corresponds to the master thesis [17], designated under the codename WP1.A3.NTNU.Thesis3. Table 13 provides a summary of the bibliographical details for this document, outlining essential information for reference.

Table 13: Bibliographical information for WP1.A3.NTNU.Thesis3

Title:	Machine learning-assisted structural health monitoring of Herøysund Bridge
Author(s):	Erling Nordli Husøy, Emil Hæreid Steen
Date:	June 2024
Language:	English
Codename:	WP1.A3.NTNU.Thesis3
Link:	https://ntnuopen.ntnu.no/ntnu-xmlui/handle/11250/3156765

The thesis aims to develop a Machine Learning (ML) algorithm to predict strain development induced by weather conditions. Alongside the ML model, the Herøysund Bridge is analysed using Finite Element Analysis (FEA) software. Simulated damage is applied to the FEA model to explore how it could aid in evaluating the potential implementation of a Structural Health Monitoring (SHM) system for the bridge. The combination of ML, the FEA model, and sensor data is used to assess the feasibility of such a system.

After developing ML models, the results show that the dataset is adequate for ML implementation, although there are areas that could benefit from improvement. In the case of a sudden loss of post-tensioning in the FEA model, the strains increased by 132.5 µm/m. In comparison, the expected error in the ML predictions of strain development due to external weather conditions, with 99% accuracy, was 46.8 µm/m. Since the expected error is significantly smaller than the strain response, these findings suggest that the ML model would effectively detect a sudden loss in post-tensioning force, should similar damage occur in the real-world bridge.

The FEA also provided valuable insights into the thermal effects within the structure, enhancing the understanding of the bridge's behaviour, as well as the sensor data. It clarified the substantial variation in measured strain response between the north and south sides of the bridge, which is attributed to solar radiation. By combining FEA with ML techniques, the study

offers a comprehensive approach to interpreting strain responses, thereby advancing the potential for an effective SHM system implementation on concrete structures such as the Herøysund Bridge.

This work investigates the use of Machine Learning (ML) to predict the impact of ambient temperature on the structural responses of the Herøysund Bridge. It shows that the temperature effects can be removed from the sensor data, allowing for the identification of features potentially indicative of damage. The study begins by reviewing simple techniques to compensate for temperature effects, such as linear regression, moving average, and autoregressive models. These simpler models serve as baseline approaches, providing a foundation to assess improvements in performance through more advanced ML techniques. Additionally, the work includes an exploration of the thermal properties of concrete, followed by an overview of ML fundamentals and concepts. To evaluate the effectiveness of the predictions, various statistical methods are employed to assess model performance.

The work is divided into two distinct approaches. One approach works directly with the measured data, aiming to analyse and predict the temperature effects on the structural responses. The other approach utilises the available numerical model of the bridge to simulate the temperature loading, allowing for an exploration of how temperature impacts the bridge's behaviour.

A significant amount of work was required to obtain, process, clean, and reformat the strain signals. Following this, the analysis of the strain data revealed considerable temperature dependencies across different sensors, as shown in Figure 36. The study suggests that this difference may be attributed to the sensor's location, specifically whether it is positioned on the north beam or the beam facing the south. The discrepancy is likely due to the increased solar radiation affecting the south side of the bridge.

(a)

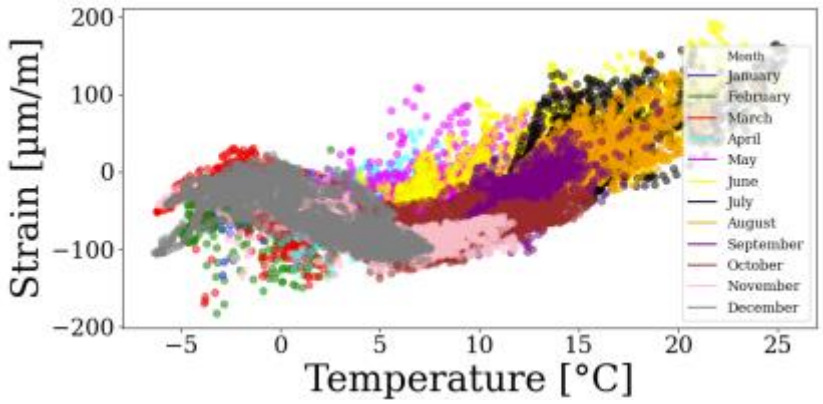

(b)

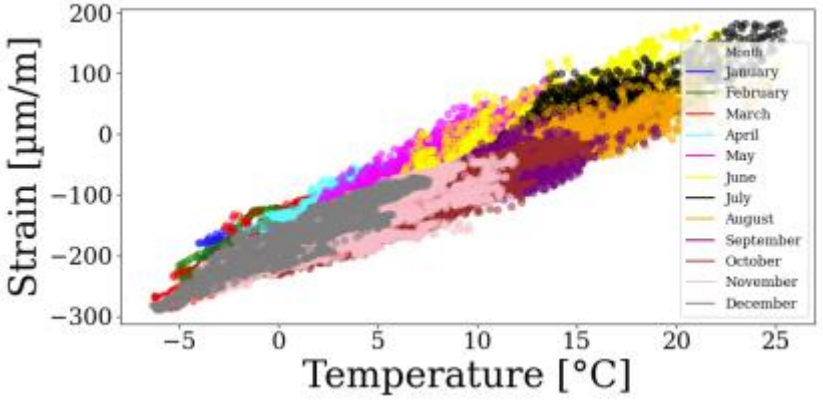

Figure 36: Monthly strain and temperature relation; (a) Sensor Point_1_N (North); (b) Sensor Point_6_S (South) (Source: [17])

The work offers a detailed description and Python scripts for loading and processing the strain signals, including methods for capturing seasonal patterns. It covers steps such as partitioning, windowing, and normalizing the dataset to prepare it for training, validation, and prediction in a Machine Learning (ML) model. Several ML architectures are considered and tuned throughout the study. The work also provides references and necessary guidelines to replicate the process using publicly available Python libraries. After training the models with the available data, the ML models are employed to predict the bridge's response. The performance of the ML models is influenced by the sensor location, with predictions from the south-side (Figure 37(b)) sensor showing better accuracy compared to those from the north-side sensor (Figure 37(a)).

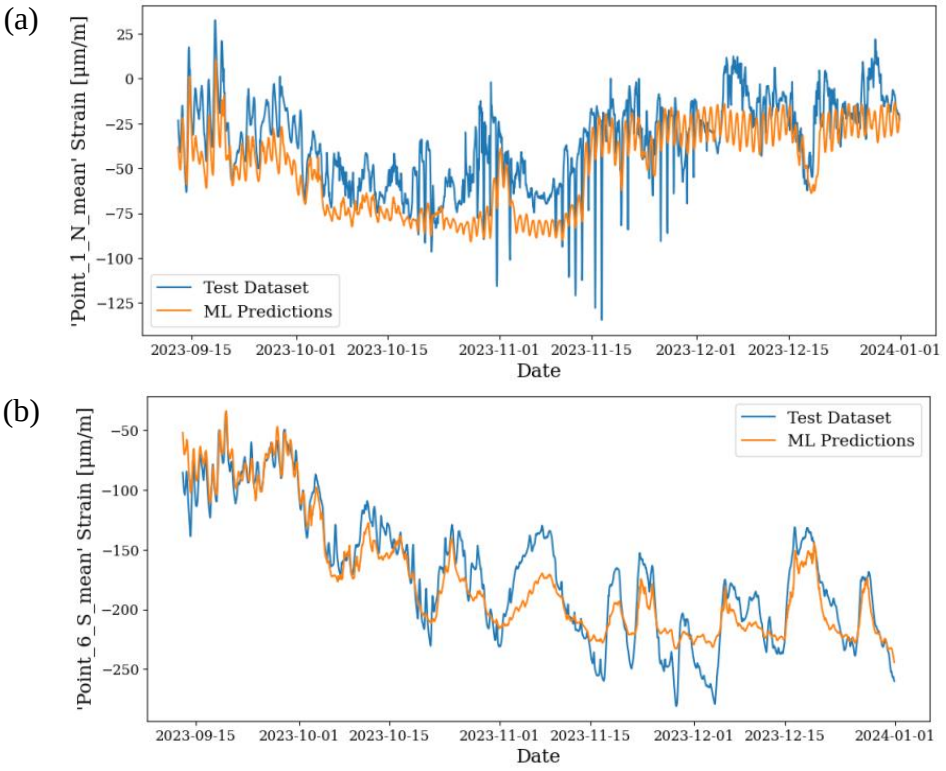

Figure 37: Comparison of measured data to ML model predictions for; (a) Sensor Point_1_N (North); (b) Sensor Point_6_S (South) (Source: [17])

In the second part of the work, the bridge is investigated numerically, with the effect of temperature validated by comparing the simulation results to the measured strain data. The work reports varying degrees of accuracy, but overall, the numerical model exhibits behaviour similar to the measured strains, as illustrated in Figure 38.

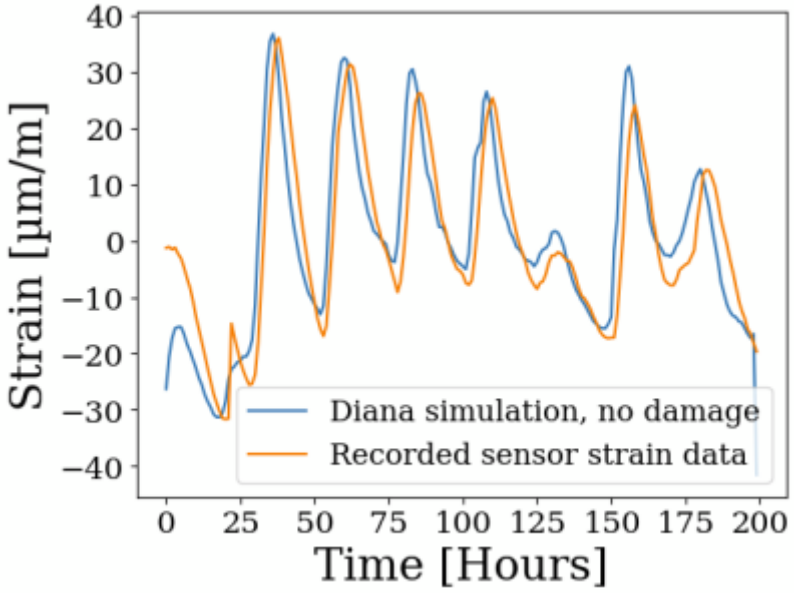

Figure 38: Comparison of simulated and recorded strain signals (Sensor Point_1_N) (Source: [17])

The numerical model can then be used to simulate damage by removing one tendon, allowing for the application of the same machine learning (ML) techniques with the numerically generated signals. By simulating damage and comparing the results with the expected error of the ML model, it is possible to assess the feasibility of detecting damage using a Structural Health Monitoring (SHM) system. Errors that deviate from the expected range could suggest that strains are influenced by factors beyond the usual extrapolation of labels, such as temperature and weather conditions. Specifically, if the error falls and remains outside this range, it could indicate alterations in strain due to structural damage or other external factors. However, if the error temporarily deviates from the expected range but then returns, this would not necessarily imply structural damage.

This idea is exemplified below. The simulated bridge damage was carried out by removing the prestressing force induced by one tendon. The simulations revealed an increase in strain of 132.5 µm/m at one of the sensor locations. Given that the expected error for the south-side model has a 99% confidence interval of 46.98 µm/m, it is reasonable to conclude that such damage can be detected within this confidence interval. This result is illustrated in Figure 39.

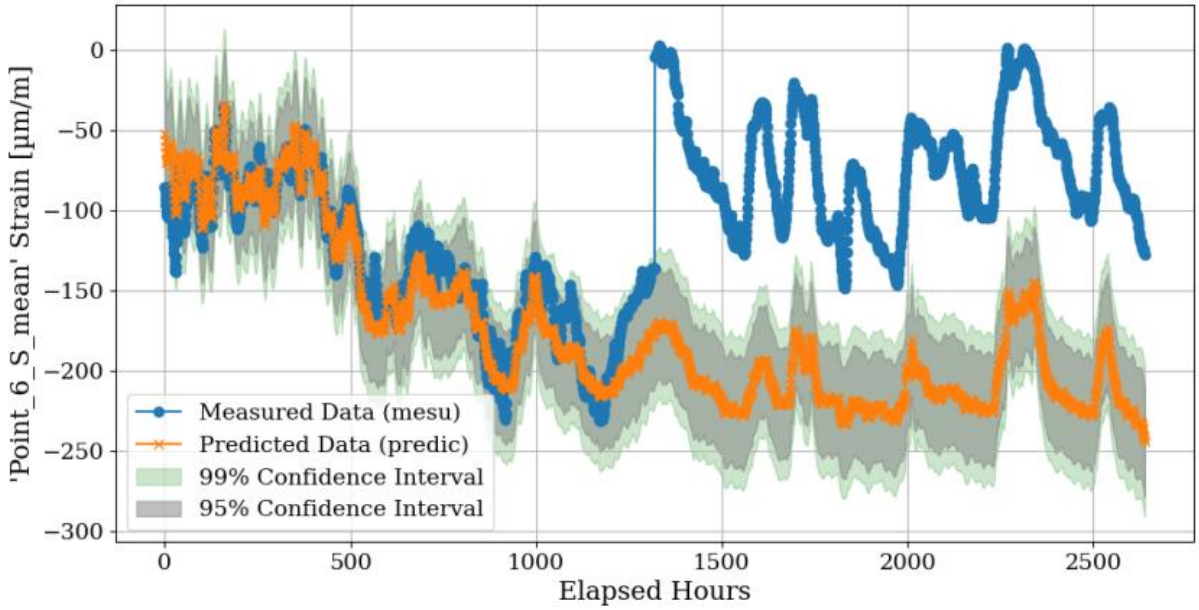

Figure 39: Simulated strain with a sudden loss of a tendon, compared against ML predictions and corresponding confidence intervals. (Source: [17])

This work concludes that significant effort is required to pre-process the sensor data to ensure its quality. It was noted that better weather tracking capabilities within the dataset could have enhanced the performance of the Machine Learning (ML) model. Additionally, there are indications of a non-symmetrical structural effect across the bridge's cross-section due to differing solar radiation exposures. This suggests that input variables should have been gathered closer to the bridge to make the dataset more suitable for ML analysis. The developed ML model outperformed the most relevant baselines, particularly for the northern sensor location. While using real-world data complicated the methodology, the study demonstrated that it was feasible within the ML pipeline.

Numerically, the research demonstrated that it is possible to detect short-term damage in a Structural Health Monitoring (SHM) system by combining Finite Element Analysis (FEA) and ML results. The strain response caused by the simulated damage was more significant than the expected error, indicating that the algorithm could effectively recognize this damage scenario.

The results suggest that an SHM system can be implemented using ML, but further research is needed to confirm the practical application of ML in operational SHM systems. Moreover, more precise weather data would contribute to improved ML performance.

5. Additional numerical investigations

This section builds on previous studies by developing a numerical model to simulate the response of the Herøysund Bridge. The model was developed and updated to accurately reflect the real bridge response and is implemented using the open-source tool VBI-2D [18]. With this framework the bridge is represented as a finite element beam model with defined boundary conditions and element properties, in Matalb. The model is used to simulate the passage of vehicles and to obtain the quasi-static responses of the Herøysund bridge. With this numerical tool and model, the primary objective is to explore the effect of damage in the post-tensioning system.

5.1. Model development and updating

The Herøysund Bridge is modelled as a 3-span continuous bridge (Figure 40), with simple supports at the ends and supports with rotational stiffness representing the columns. The Matlab modelling incorporates several assumptions to simplify the representation: the bridge geometry is considered flat, there is only one tendon geometry, and no variation of prestress force (P) in space. Additionally, the model assumes no change in the centroid location when damage is introduced, as the variation and effect are very small. Ordinary reinforcement is not included, and the structure is modelled using beam elements. While the model does not perfectly replicate the exact geometry (particularly near the supports, where changes from box to beam cross-sections occur) and it uses a simplified tendon layout, the representation is deemed appropriate for parametric investigations.

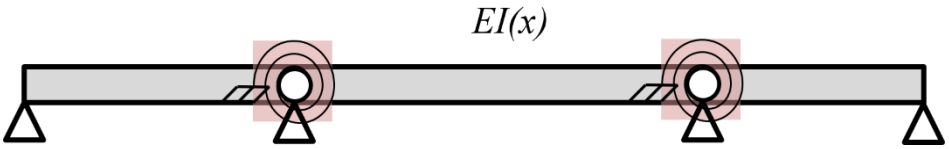

Figure 40: Herøysund Bridge model in VBI-2D tool

The geometry of the prestressing system is obtained from the drawings of the original construction project of the bridge. Due to the complexity of the tendon geometry, it was considered appropriate to approximate it. Each beam in the model has four tendons, each with a different geometry. However, in the numerical model, it is assumed that all four tendons are located at the same vertical position along the beam. This simplification is illustrated in Figure 41.

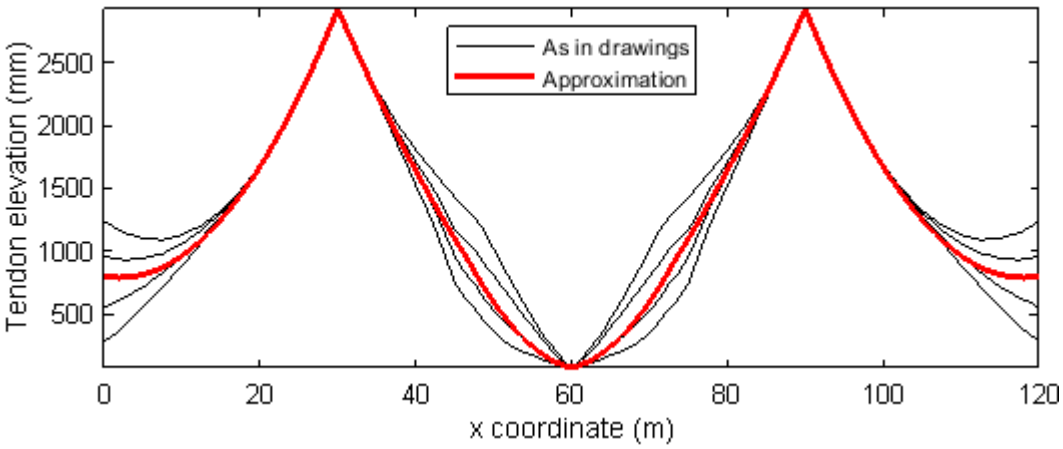

Figure 41: Geometry of tendons as in drawings and for VBI-2D model.

Similarly, the section properties along the beam are modelled based on the bridge's geometry, which was extracted from the available drawings in the Brutus system. Using this information, the second moment of area at each location along the bridge is calculated and incorporated into the numerical model. This allows for the determination of the transformed cross-section, as shown in Figure 42.

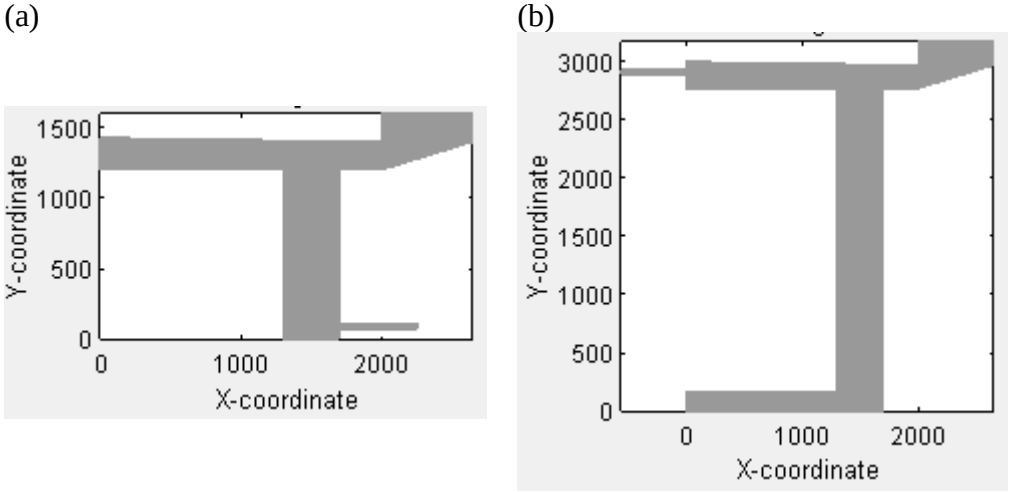

Figure 42: Transformed cross-sections; (a) Mid-span; (b) At columns

The final distribution of the second moment of area along the beam model is shown in Figure 43. This property was calculated for the case with all tendons included. Drastic variations in magnitude are observed, primarily due to the varying depth of the bridge's cross-section. Additionally, sudden jumps can be seen, corresponding to the transition between different types of cross-sections (from open to closed). It is important to note that the real bridge features a gradual transition between these two types, which was not incorporated in this simplified model. The study is repeated for cases where tendons are missing in the cross-section. The results, presented as relative variations with respect to the undamaged case, are shown in Figure 43(b). The effect of a missing tendon leads to only a marginal reduction in local stiffness. The maximum reduction occurs at mid-span, with an approximate decrease of 1% for each tendon missing.

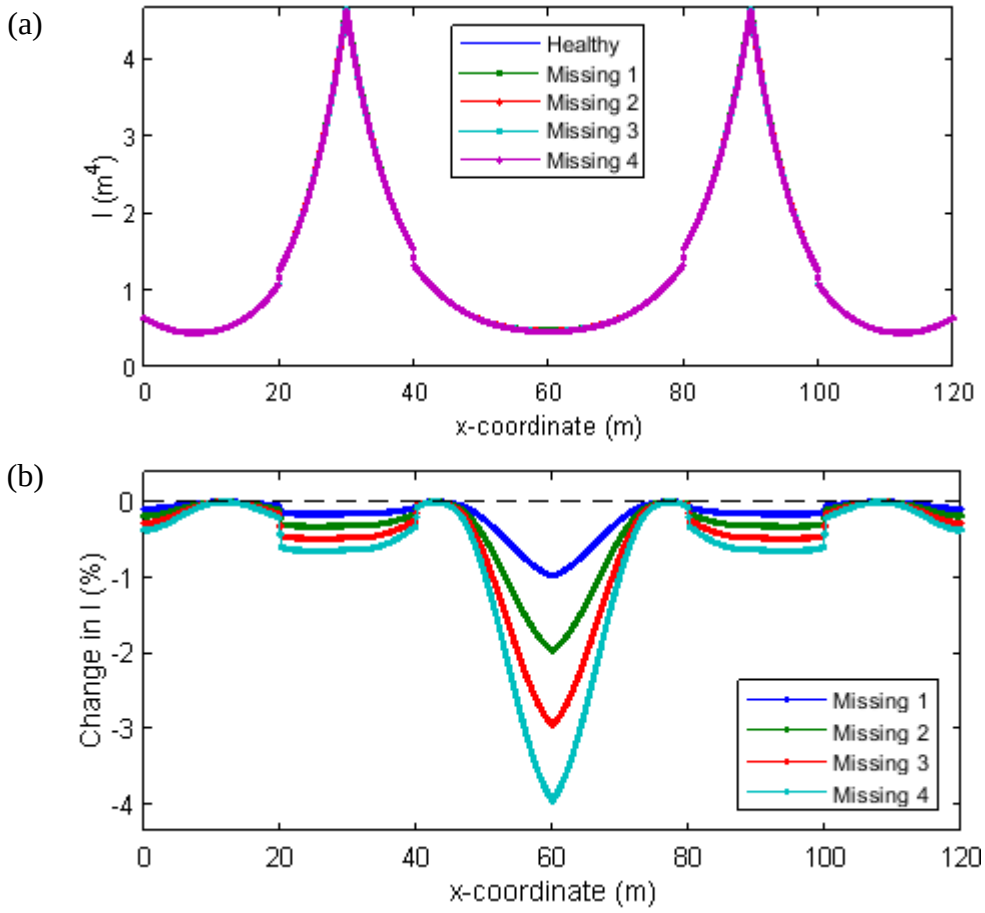

Figure 43: Second moment of area along the beam in VBI-2D; (a) Values of different number of missing tendons; (b) Relative variation with respect to undamaged case.

The final properties of the numerical model were determined through model updating, which involved fine-tuning the mass and the elastic modulus of the beam using appropriate factors, as well as adjusting the rotational stiffnesses of the supports to accurately represent the columns. This was accomplished by referencing the mid-span deformation of 33 mm observed during a 50-tonne truck calibration event conducted prior to the project's start, as reported in [15]. However, due to uncertainties in the actual axle weight, a deformation of 30 mm was adopted for the model. Additionally, the model was adjusted to match the frequencies reported in [19] (1.44, 2.39, 3.57 Hz) and [20] (1.37, 2.41, 3.76 Hz), which correspond to the first three vertical bending modes observed using a 3D model. Since VBI-2D is a 2D model, some differences were expected. The final numerical model resulted in a mid-span deformation of 30 mm and frequencies of 1.30, 2.69, and 3.60 Hz.

Due to the simplifications in the model, achieving an exact match between the numerical and measured responses is challenging. Despite this, the strain response for calibration Day 1 is compared below in Figure 44. The responses do not match perfectly, which can be attributed to several factors. Firstly, the numerical model is a simplified representation of the bridge. Additionally, the exact entry and exit times of the vehicle are unknown. The strain on the bridge is measured on the carbon fibre strip, and these measurements include dynamic effects and noise. The recorded strain also needs to be normalized, as it is influenced by the sensor factor, and the fact that the sensor is attached to the carbon fibre plate, effectively measuring a longer strain than modelled numerically. Given these circumstances, the numerical model was considered appropriate for representing the bridge and studying the effect of damage.

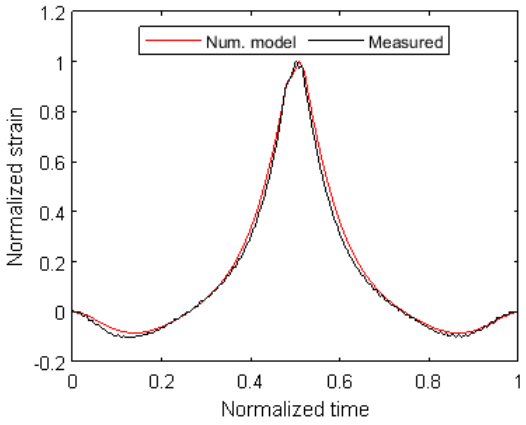

Figure 44: Comparison between measured and simulated normalized strain response for calibration Day 1 at mid-span

5.2. Effect of damage

In the VBI-2D model of the Herøysund Bridge, damage is represented in the following ways:

- Equivalent upward forces are applied at the corresponding nodes of the affected elements.
- Additional moments are introduced at the ends of the damaged sections.
- Changes in section properties are accounted for due to the loss of steel, representing the effect of the missing tendons.

The numerical model was verified through two tests:

- Verification 1: A simply supported beam with a straight tendon and part of the tendon missing. This verification validated the effect of additional moments at the ends of the damage.
- Verification 2: A parabolic tendon with no end eccentricity and the full tendon missing. This test validated the effect of additional upward forces due to the prestress geometry.

With the verified, validated, and simplified numerical model, damage scenarios were simulated, as outlined in [21], yielding similar results. This model is now used for a parametric study on damage at mid-span, specifically focusing on a single missing tendon. The study explores the impact of different damage lengths on static strain values, measured at different locations along the structure. The results, shown in Figure 45(a), reveal complex relationships due to the variation in the structure's bending stiffness (*EI*). In particular, Figure 45(b) illustrates the static strain values measured at mid-span, highlighting the intricate effect of damage length.

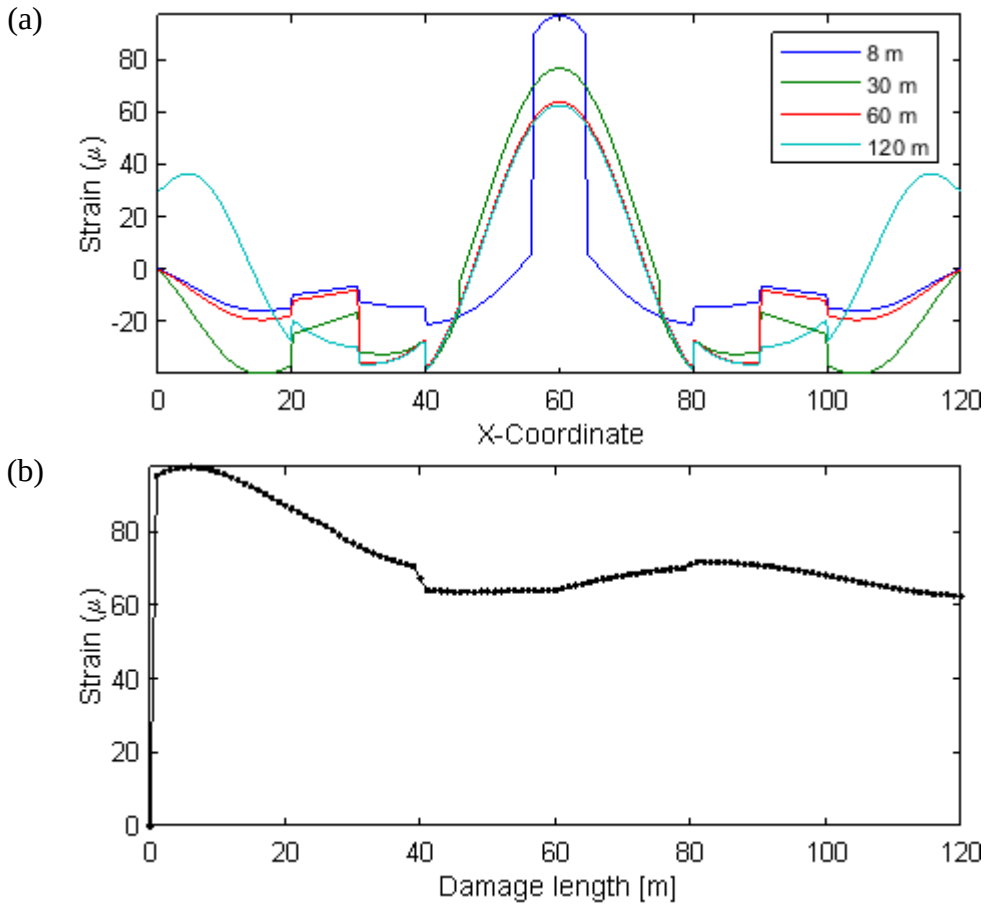

Figure 45: Static strain for mid-span tendon damage; (a) Effect of damage length for different sensor locations; (b) Effect of damage length for a sensor at mid-span.

For completeness, the same parametric study was repeated, this time focusing on the vertical deformation in Figure 46.

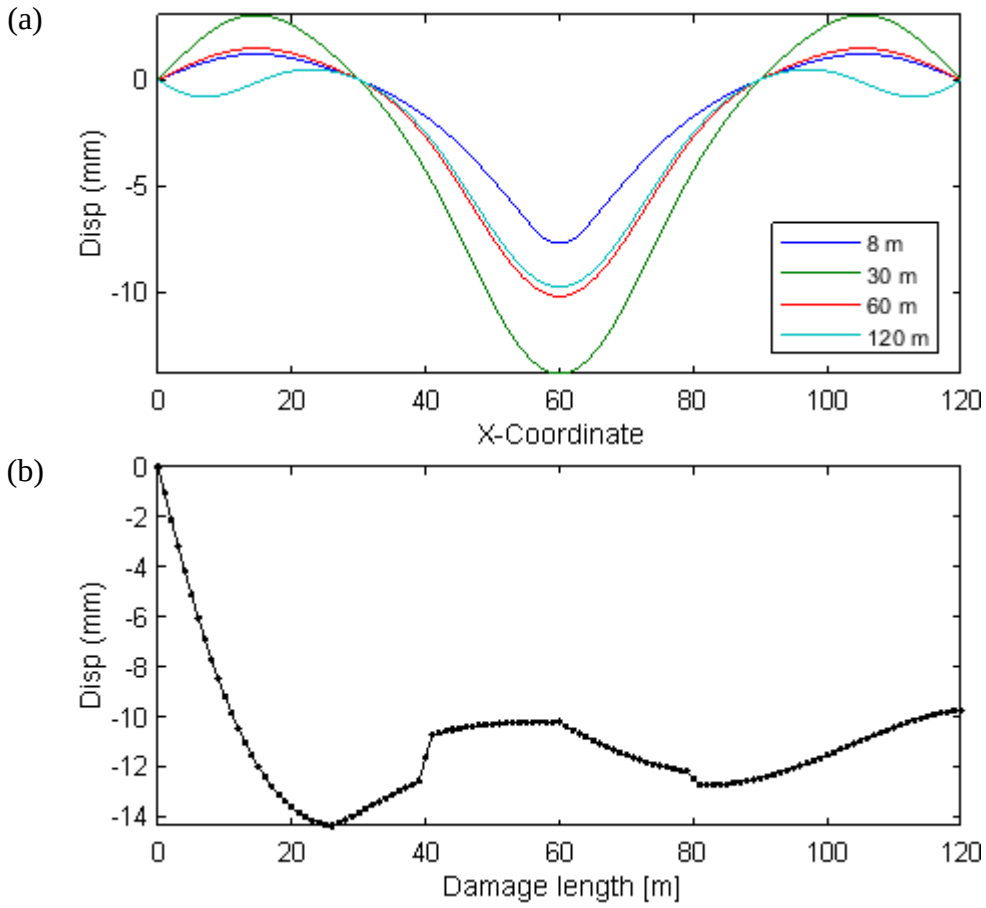

Figure 46: Static vertical displacement for mid-span tendon damage; (a) Effect of damage length for different measuring locations; (b) Effect of damage length for displacements at mid-span.

Regarding the quasi-static component, damages result in changes to the shape of the influence line. For the case of a 1% stiffness reduction, the corresponding errors in GVW are shown in Table 14. While the reported errors are relatively small, they are of the same order of magnitude as the reduction in stiffness. Different sensor locations may exhibit varying sensitivities to these changes. Additionally, the error varies with the length of the damage, but it is not proportional. As shown in Table 14, the smallest error occurs for a damage length of 30 m, while shorter lengths of damage tend to cause larger errors.

Table 14: GVW error a mid-span for a 1% stiffness reduction

Length of damage (m):	8	30	60	120
GVW error(%):	0.7941	0.5489	0.8273	0.9172

Clearly, further work and investigations are required. This study opens up new possibilities for monitoring, particularly in terms of assessing the bridge's condition. Although the errors in GVW are small, they could still serve as a valuable resource for evaluating structural health. In fact, these errors may be more sensitive to damage than traditional modal properties, offering an alternative approach for damage detection and monitoring.

6. Additional analysis of measurements

To complement the previously reported analysis and results, this section presents additional investigations using the actual measurements recorded throughout the duration of the project. The focus of the analysis is on the effect of temperature on the structural response and how this can be processed to detect potential damages in the bridge. Furthermore, the results from the calibration runs, as reported in Section 3.4, are utilized to estimate the Gross Vehicle Weight (GVW) of all heavy traffic over the four-year period.

6.1. Effect of temperature

6.1.1. Example effect of temperature

The effect of temperature on the strain signals is considerable, as demonstrated by the records from a single day, shown in Figure 47. This figure presents example signals over a 24-hour period, derived from a combination of 24 files. While the measured temperature fluctuated somewhat, these changes were not overly dramatic. However, the measured strain displayed significant variations, particularly in the static strain. These variations must be related to the ambient loading but cannot be correlated with temperature in a straightforward manner. As seen in Figure 47(b), the strain signal exhibited some relatively sudden changes in its trend, approximately between 15h and 21h.

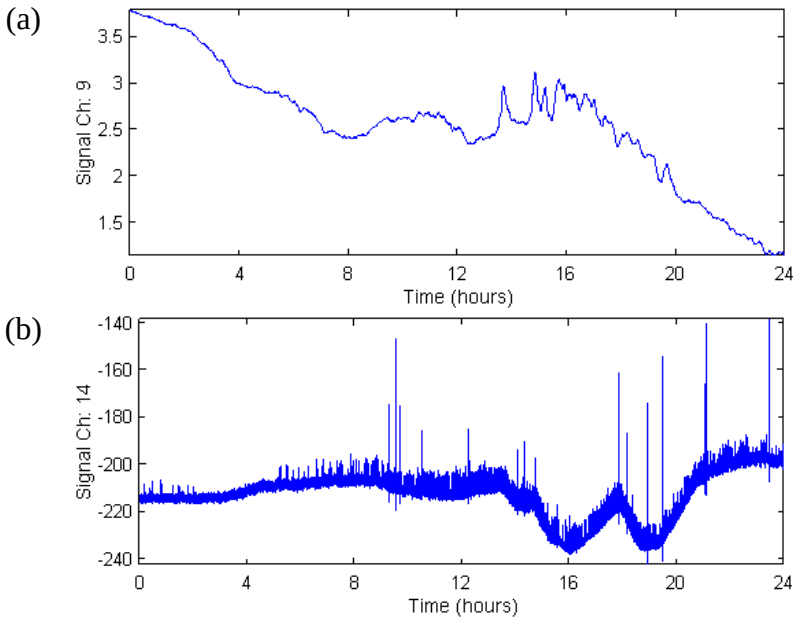

Figure 47: Full day (1st April 2024) signal record. (a) Temperature (Sensor 9); (b) Mid-span strain (Sensor 14)

The measured structural responses must be processed to account for the complex effect of temperature. However, the signals also include the quasi-static strain from vehicle passages, which manifest as large, narrow peaks in Figure 47(b). To isolate the underlying trend and correlate it with temperature, it is necessary to remove the bridge's responses when it is loaded by traffic. Since this task cannot be performed manually, an automatic procedure was developed to carry out this process.

6.1.2. Underlying trend extraction

This process is applied to each 1-hour file, where the signals contain noise and spikes caused by traffic loading. The objective is to identify segments of the signal that correspond to periods when the bridge was unloaded. Since the bridge has only one lane and traffic is regulated by traffic lights, there are multiple times each hour when the bridge is likely to be unloaded. The aim is to isolate the underlying structural behaviour influenced by temperature by analysing the trend in the responses during these unloaded periods.

To automate the detection of unloaded periods, the process is carried out using a combination of signal processing techniques. First, the signals are smoothed using a moving average filter with a 4-second window. This effectively removes signal noise while preserving the changes in the signal caused by traffic loading. Next, the first time derivative of the signal is calculated. Values close to zero indicate that the signal has little to no slope over time, suggesting that the bridge response is not changing, and the bridge is likely unloaded. The signal is then divided into 2-minute segments, and within each segment, the time with the first time derivative closest to zero is taken as the reference value. These reference values from each segment (one every 2 minutes) are combined to form the underlying trend of the bridge response. This procedure assumes that temperature variations occur gradually over time.

As an example, Figure 48 demonstrates the application of this procedure to a 1-hour signal. Using this method, we can isolate the signal that represents only the effects of traffic load by removing the temperature-related trend. The red line in the figure shows the underlying behaviour of the structure, which reflects the influence of temperature. By compensating for temperature effects and removing this trend, we are left with the strain signal that corresponds solely to the traffic load on the bridge. This allows us to focus on the strain caused by the vehicle passages, with the static strain representing the response of an unloaded bridge.

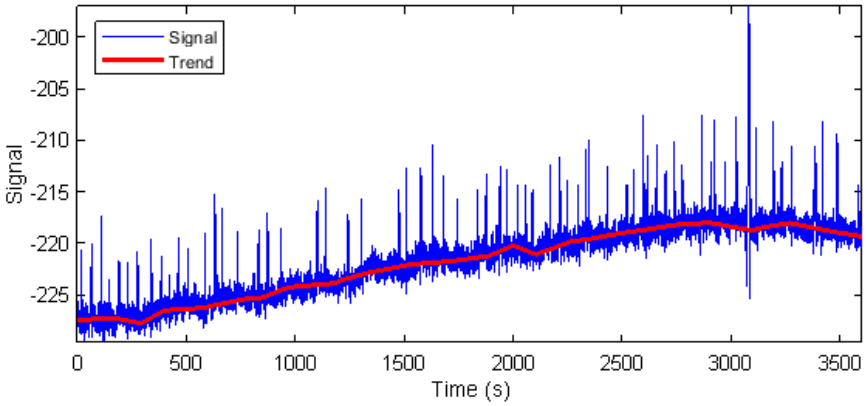

Figure 48: Example of temperature trend extraction for file 20240401170038.

For the same strain signal, if we include a sudden change in strain, it would look like the signal shown in Figure 49. This is the same signal as in Figure 48, but with an additional sudden increase of 20 μ-strain. This sudden change would appear as a sharp deviation in the static strain response, superimposed on the underlying trend caused by temperature fluctuations. The spike in strain could indicate an unusual event or potential structural damage.

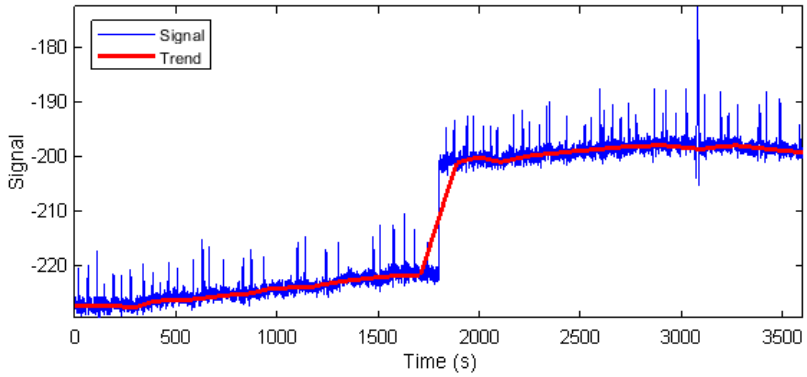

Figure 49: Example of signal and temperature trend, including a sudden change in strain.

6.1.3. Anomalies in underlying trend

To identify possible sudden jumps in the underlying temperature trend, the database was explored to locate the files with the largest jumps. For instance, this analysis was conducted for the strain signal recorded by Channel 14 (mid-span). The top 40 files showing the most significant jumps were examined in detail. This investigation revealed multiple potential causes for these large jumps, which were categorized and codenamed as follows:

- Veh (Slow vehicle): Jumps caused by a slow-moving vehicle passing over the bridge.
- SP (Signal Processing): Issues related to signal processing errors.
- JD (Jumping Drift): Sudden changes in strain values that either eventually return to the trend or result in values becoming "stuck."
- TV (Large Temperature Variations): Cases where the underlying trend shifts significantly due to rapid temperature changes.

These findings highlight the need for careful signal interpretation to distinguish between structural responses and other influencing factors.

Most of these deviations can be addressed or accurately identified using a refined methodology:

- Slow Vehicles: These exhibit distinct patterns where the strain signal dips below, rises above, and then falls below the temperature trend, as shown in Figure 50(a)
- Signal Processing: Figure 50(b). These issues can be resolved by revising and improving the algorithm to handle anomalies more effectively.
- JD (Jumping Drift): Such jumps generally revert to the trend after some time, allowing for identification and adjustment (See Figure 50(c)).
- TV (Large Temperature Variations): These can be corrected by evaluating the overall smoothness of the trend, rather than focusing solely on the transitions between segments (See Figure 50(d)).

Refining these approaches will enhance the reliability of the signal analysis and better separate the effects of temperature and traffic loading.

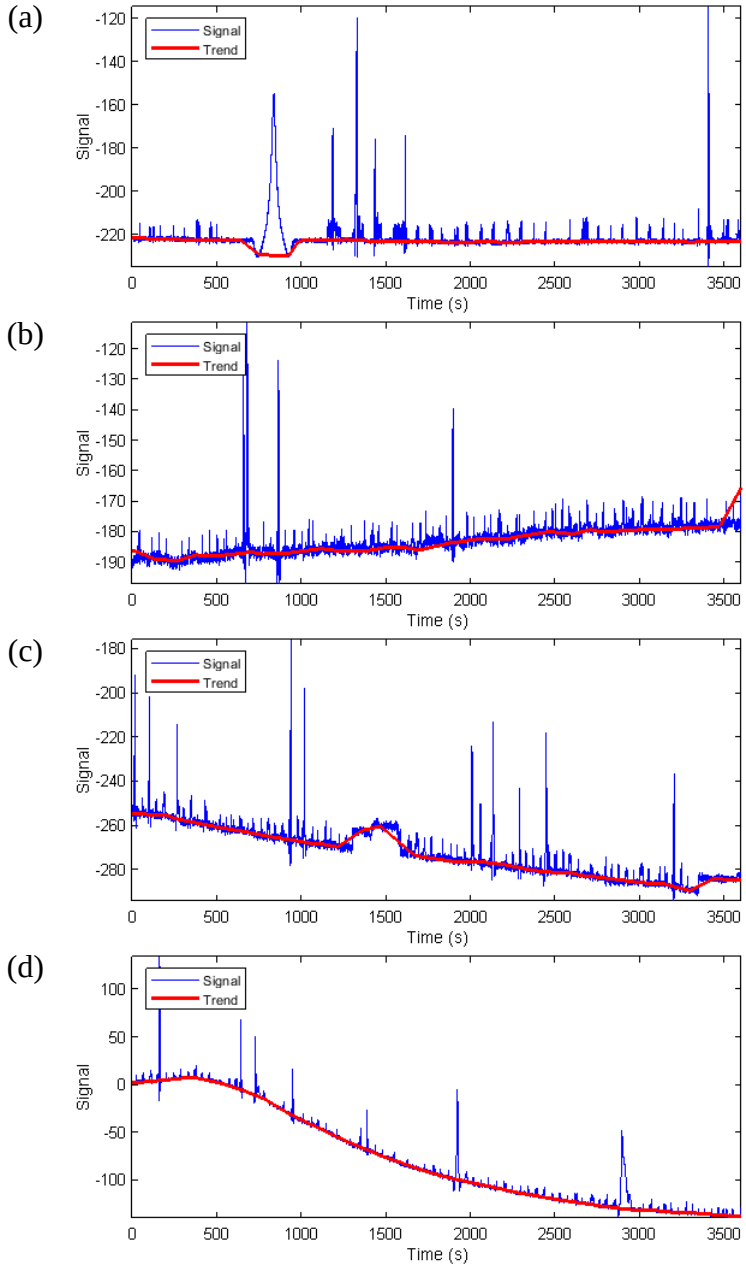

Figure 50: Examples of larger deviations in temperature trends; (a) Slow vehicle; (b) Signal processing issue; (c) Jumping drift in sensor; (d) Large temperature effect

Regarding the JD cases, it was initially believed that these occurrences were sensor specific. However, upon closer examination it was discovered that such jumps appear not only at a single sensor location but across multiple sensors (though not necessarily all). This finding suggests that the phenomenon might reflect a sudden change in the structural behaviour of the bridge. The figure below illustrates the trends for all strain gauges corresponding to the same file shown in Figure 50(c). No possible explanation can be offered at this point on exactly what cases this jump in the signal or what can possibly affect the structural behaviour in this manner.

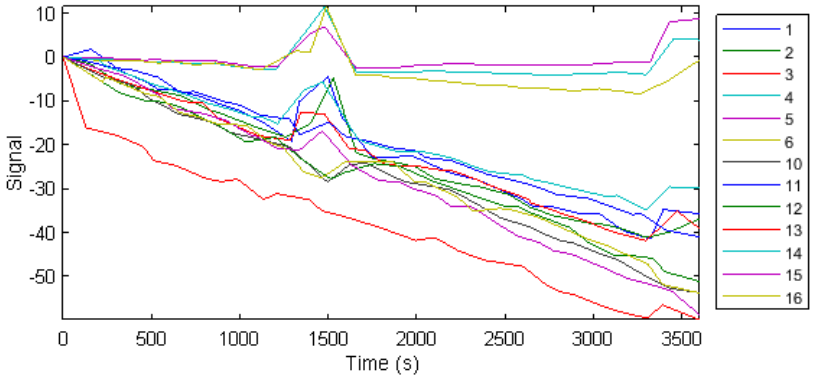

Figure 51: All temperature trends for all strain gauges (file: 202402061256)

Among the Top-40 cases analysed, one file exhibited an especially suspicious signal, as shown in Figure 52. Over the course of 300 seconds, there was a drastic and sharp change in strain trend. This anomaly was recorded in file 202401311354. Interestingly, this abrupt change was not observed in all sensors, raising further questions about its origin. The recorded temperature variation during this hour was minimal, with a total fluctuation of less than 1 degree. Given the lack of correlation with temperature and the inconsistency across sensors, this particular instance remains unexplained.

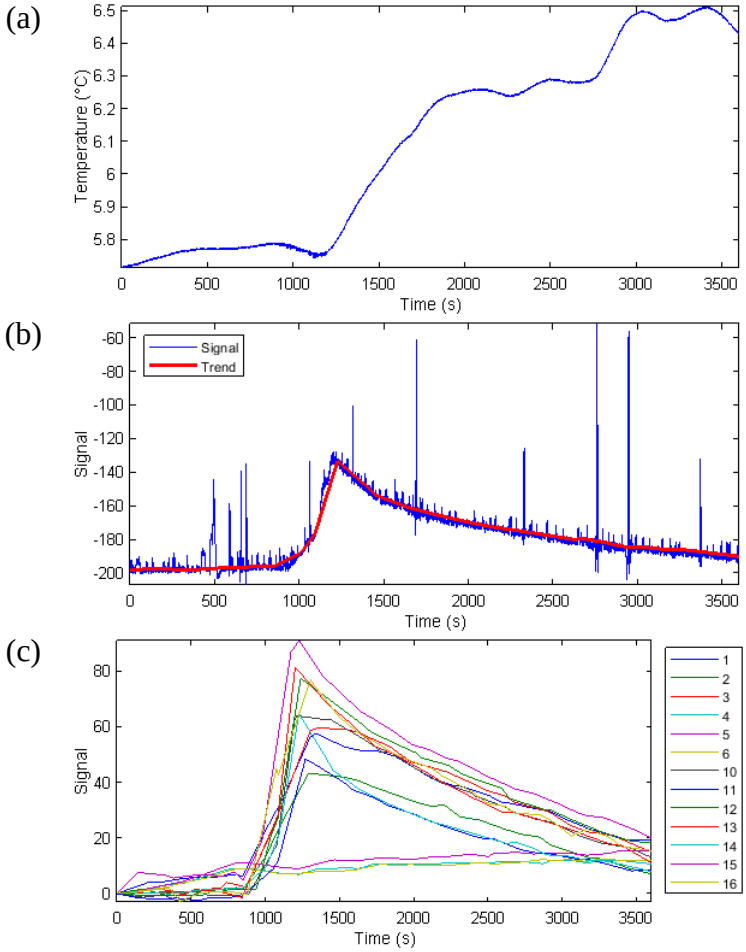

Figure 52: Suspicious case; (a) Strain signal and underlying trend for Channel 14. (b) Underlying trends for all strain sensors

6.1.4. Temperature effect in dataset

Once the underlying trend is determined, the effect of temperature can be further explored. For the dataset of 30 406 files, an average temperature can be calculated for each time period and compared to the corresponding average strain. Typically, the underlying strain value within an hour changes only slightly, making the average strain a reliable representative value for analysis each 1-hour file.

While some files exhibit significant strain variations due to issues such as slow traffic, poor signal processing, or jumping drifts, these problematic cases represent only a small fraction of the total dataset. Thus, the vast majority of files provide consistent and valid data for studying the relationship between temperature and strain.

Refer to Figure 53, which presents the static average strain values. Each dot in the figure represents the result derived from a 1-hour file, with the colouring corresponding to the time of measurement. The strain values are shown for a selection of 4 sensors, highlighting variations across different locations:

- Ch. 1: Original installation on the North beam (x = +640 mm)
- Ch. 4: Original installation on the South beam (x = -940 mm)
- Ch. 10: New installation on the North beam (x = -15 000 mm)
- Ch. 14: New installation on the South beam (x = 0 mm)

These strain values illustrate the response at various sensor locations, providing insight into the structural behaviour over time and across different beam positions.

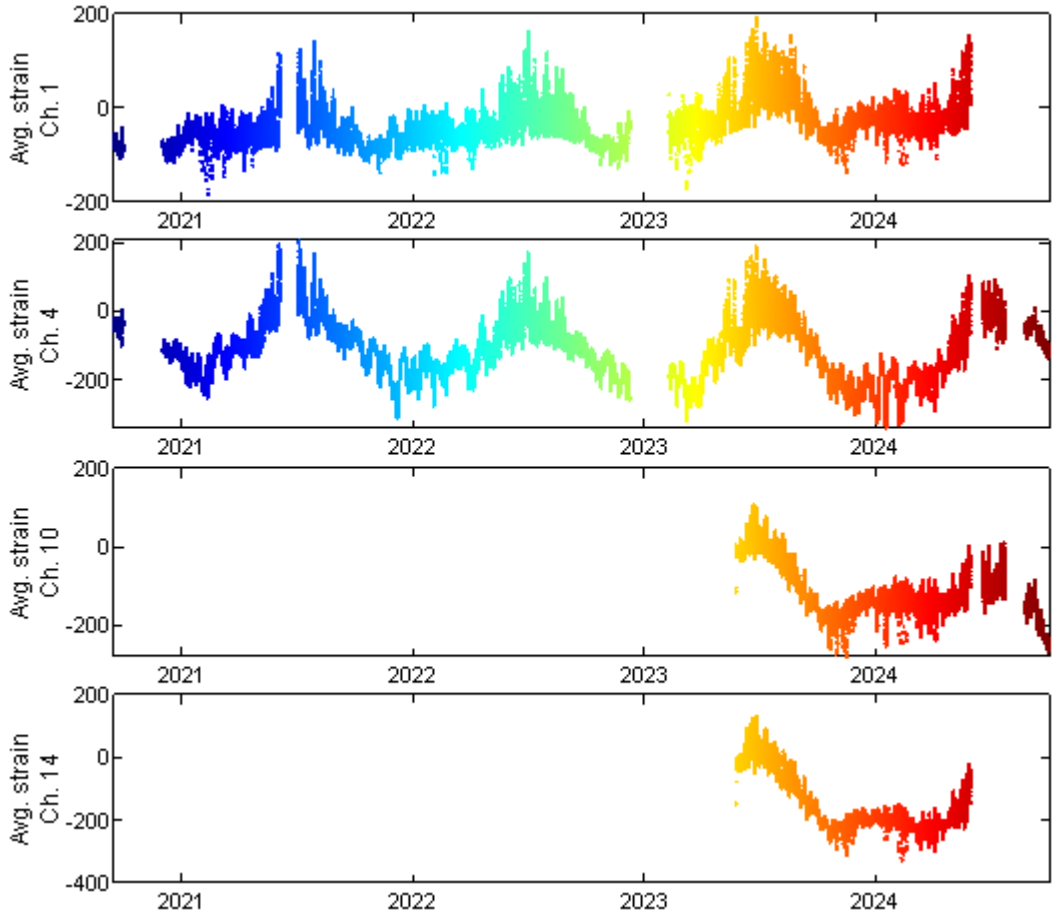

Figure 53: Average strain for each 1-hour file for a selection of channels. The colouring is proportional to time of measurement.

Figure 54, using the same colouring scheme as Figure 53, highlights the relation between temperature and strain. Sensor 1 exhibits a pronounced non-linear behaviour, particularly evident around the freezing point. In contrast, Sensor 4 shows a much clearer linear relationship with temperature. Initially, this suggested that the observed non-linearity might depend on the beam where the sensor was installed. However, further analysis with the newer strain gauges, such as Sensors 10 and 14, reveals that both, despite being installed on the North and South beams respectively, display a strong non-linear relationship. This indicates that the non-linearity is not solely determined by the beam location of the sensor.

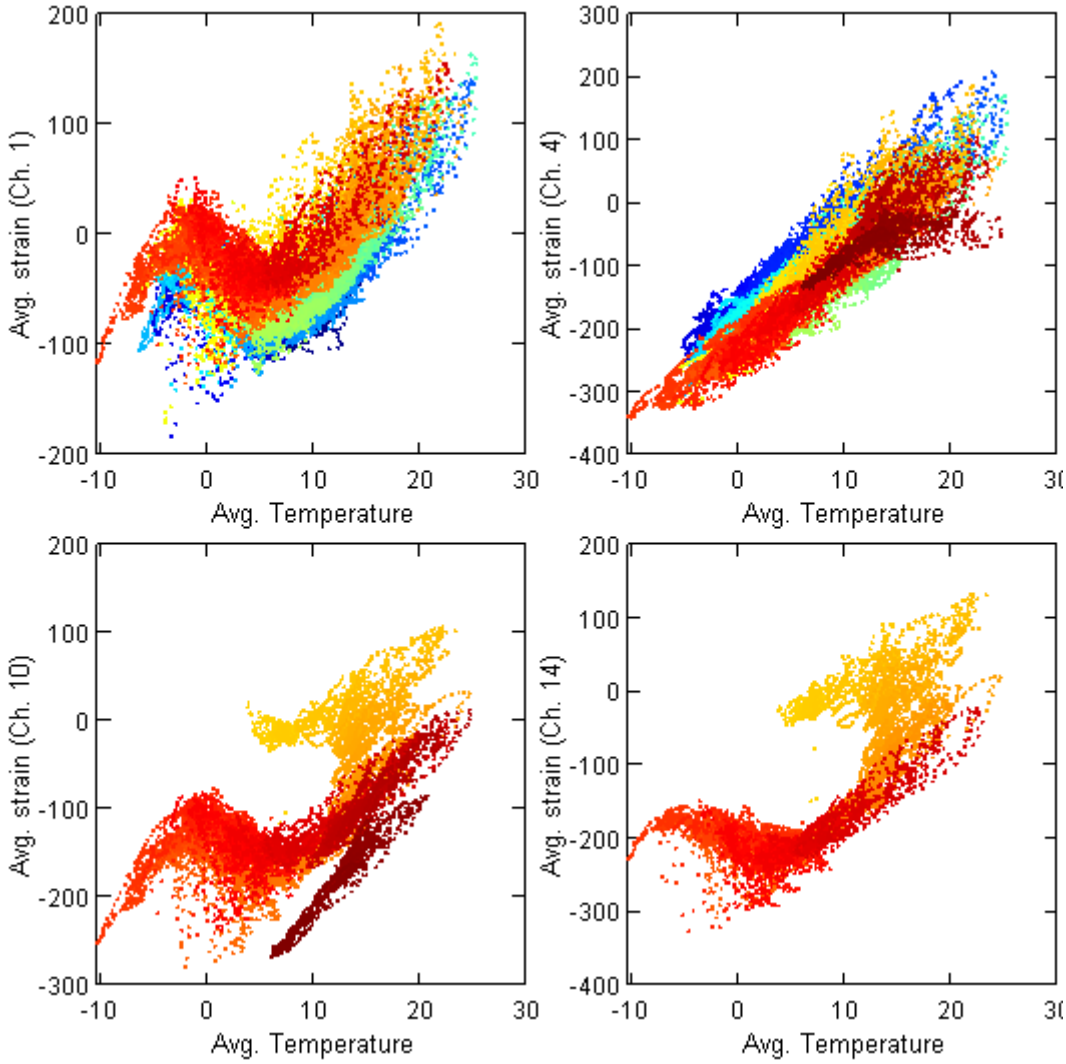

Figure 54: Relation between average static strain and temperature for a selection of channels. The colouring is proportional to time of measurement.

6.2. GVW estimation

Using the outlined tools and obtained factors in Section 3.4, it is now possible to estimate the GVW. Initially, the analysis is conducted for the calibration events, where the vehicle weights are known, allowing for an assessment of the accuracy of the calculations. Following this validation, the analysis is extended to the entire dataset to estimate the GVW for all heavy vehicle events.

Calibration Day 2 corresponded to a truck with a GVW very close to the maximum allowable vehicle weight on the bridge. Consequently, the GVW factor from Day 2 was chosen for subsequent calculations. This approach ensures conservative overestimations of GVWs for vehicles exceeding the Day 2 reference weight, while underestimating GVWs for lighter vehicles. Figure 55 illustrates the GVW estimation errors for the calibration events when using the Day 2 factor. The results show that GVWs for Day 1 and Day 3 are underestimated, while the errors for Day 2 are minimal. If this factor is applied to events involving heavier vehicles, the resulting error will likely be positive, leading to an overestimation of the GVW. Although achieving zero errors in GVW estimation is ideal, the non-linear behaviour of the structure

makes this challenging. It is preferable to overestimate the load for vehicles that exceed the maximum allowed weight on the bridge.

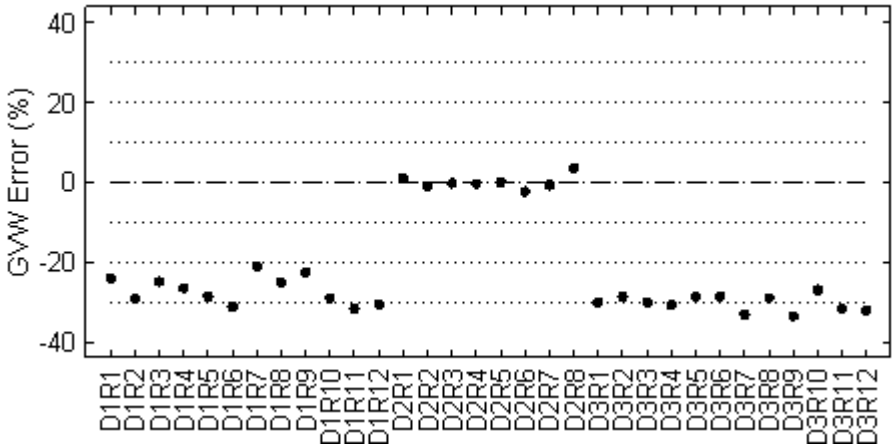

Figure 55: GVW estimates using the calibration factor for Day 2 for Channel 6. GVW estimation errors for all calibration events using the factor for Day 2.

The entire dataset is now processed. The first step is to automatically identify events, which was accomplished by detecting local maxima and extracting signal data within a 25-second time window. Not all events are considered; only those with a peak strain greater than 100 μ-strain for Channel 6 are selected. Channel 6 was chosen as the reference because it was continuously monitored throughout the measurement campaign and is located near the mid-span section of the bridge.

This process led to the identification of more than 44 000 individual events. For each event, the vehicle's speed was determined using the Convoluted Reciprocity (CR) method. The signal was then converted into the spatial domain and integrated, enabling the GVW to be calculated by multiplying the integral of the signal by the calibration factor from Day 2. The results of this analysis, which display the GVW estimates for the processed events, are shown in Figure 56.

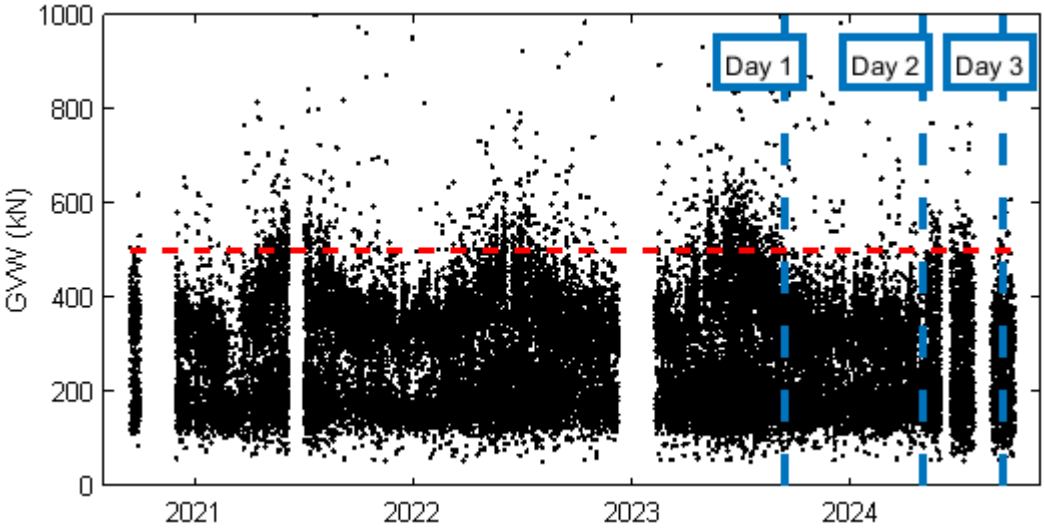

Figure 56: GVW estimates for all heavy vehicle events. Red line: Maximum allowed GVW on the bridge. Blue lines: Calibration days

The results shown in Figure 56 reveal several key insights. Firstly, the GVW estimates display a clear seasonal trend, with higher values recorded during the summer months. The data also indicates that numerous events exceed the maximum allowed weight for the bridge. A closer examination of these high GVWs revealed that they often occurred during consecutive heavy truck passages. While each truck may not have been fully loaded, the cumulative load from successive vehicles was significantly higher. This underscores the importance of considering vehicle platoons or consecutive heavy truck events, as they can cause greater load impacts on the bridge, even if each individual truck is not carrying its maximum weight.

Several of the heavier events have been examined in detail. Most of the largest GVW values correspond to situations where multiple heavy vehicles cross the bridge in quick succession. For example, Figure 57(a) depicts the event with the highest estimated GVW (+1000 kN), which results from two heavy vehicles passing closely together. A similar scenario is shown in Figure 57(b), where the trucks are spaced further apart. Despite the larger strain values, the bridge appears to be loaded by one truck at a time, with one truck leaving as the other enters.

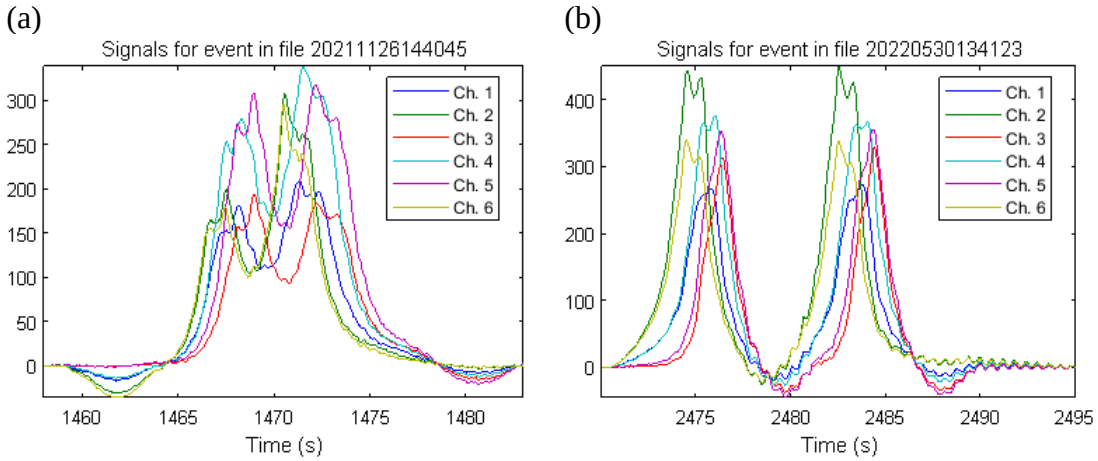

Figure 57: Examples of events giving high GVW results

However, the author acknowledges several sources of error in the analysis. A significant limitation is the lack of compensation for temperature variations, as there is insufficient calibration data to determine the precise effect of temperature on the measurements. Additionally, the automation of event definition treated each signal as a single event, which may introduce errors in cases where multiple vehicles crossed the bridge simultaneously or in quick succession, potentially affecting the accuracy of event classification. Moreover, it is unlikely that vehicles in normal traffic maintain a constant speed due to the bridge's varying slope, and this speed variation was not accounted for in the event analysis. The potential impact of these issues on the accuracy of GVW estimations remains unexamined. These factors should be considered as limitations of the study and areas for improvement in future analyses.

7. Discussion

Continuous monitoring is a widely adopted strategy for assessing the structural health of bridges, typically relying on acceleration signals. However, damages that impact the post-tension system and its prestressing force have minimal influence on the dynamic properties of bridge. Consequently, this document investigated the potential of using alternative load effects, particularly strain responses, to detect damage in post-tensioned systems. Here, damage was characterized by the breakage of a tendon and the subsequent loss of prestressing force, either locally or along the entire tendon. This study specifically explored the feasibility of establishing an early-warning system for sudden tendon breakages in post-tensioned systems, based on continuously monitored strain signals.

In addition, this work initially aimed to develop a Bridge Weigh-In-Motion (BWIM) system using the installed strain monitoring system. However, the non-linear response to traffic loads complicates the task of determining traffic weights from measured bridge responses. Standard BWIM procedures assume linear relationships, making them less effective in this context. Achieving accurate results requires more detailed and extensive calibration procedures. It is advisable to avoid employing BWIM systems on cracked prestressed concrete structures due to their inherent non-linear behaviour.

Nevertheless, the optimal solution for structural health monitoring (SHM) will not rely on a single approach. Instead, it should integrate all possible sources, methods, and concepts. Strain-based methods should complement other techniques, including the monitoring of dynamic properties. A robust SHM solution will be a blend of multiple methods, tailored to the specific characteristics of the bridge in question. Given the diversity of bridge constructions, not all methods are equally applicable to every structure. Some approaches may prove more effective for certain bridges than others. Based on the results and concepts outlined in this document, a comprehensive SHM system could be envisioned as described below.

7.1. SHM concept

It is conceivable to develop an SHM system that encompasses multiple bridges across a road network, utilising information from various sources throughout the network. By gathering data on traffic and correlating it with structural responses, valuable insights into the condition of the structures and potential damage can be obtained. This concept builds upon the vision presented in [22].

Information sources may include live traffic data, on-board sensors in heavy vehicles, pavement-based weigh-in-motion (WIM) stations, and monitoring systems installed on bridges, as conceptually shown in Figure 58. Vehicle weights can be collected or estimated and subsequently compared to the weight estimates obtained from each monitored bridge. Discrepancies in these weight estimates may signal significant changes in structural behaviour. Additionally, continuous analysis of measured bridge responses could help detect anomalies or sudden changes indicative of damage.

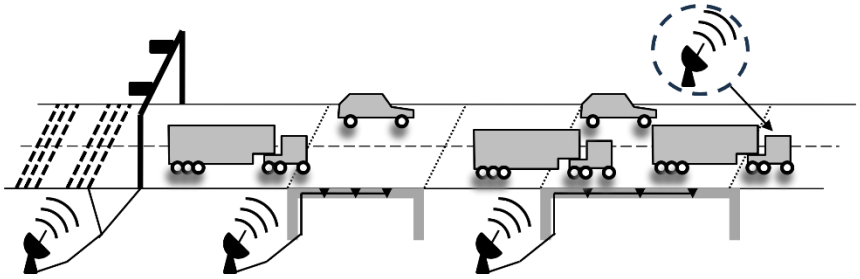

Figure 58: Conceptual representation of SHM based on information gathered from various sources across the road network.

Once a reference value for the Gross Vehicle Weight (GVW) is established, it can be compared to the estimated value derived from bridge monitoring systems. The results in this report and past research indicates that errors in GVW estimation are directly linked to changes in structural stiffness. Expected variations in these errors, stemming from noise and dynamic effects in real measurements, can be mitigated by averaging values over specific periods, such as daily averages.

Additionally, when more detailed information is available from passing vehicles, such as axle weights and spacing, it becomes possible to extract the Influence Line (IL) for each passage. Damage to the structure will be reflected in the IL, but this method is more sensitive to noise and dynamic effects. To obtain a reliable IL and detect any deviations indicative of damage, data from a significantly larger number of vehicle passages is required.

On the other hand, utilizing information from multiple sources across various locations offers the advantage of enabling accurate calibration of the monitoring systems. This multi-source data can help compensate for temperature effects and account for the non-linear behaviour of structures, ensuring more reliable assessments of their condition.

8. Conclusion

This document has examined the potential of employing strain signals for structural health monitoring, focusing on detecting sudden breakages in post-tension systems. The investigation included numerical studies using several independent bridge models. Additionally, real signals recorded from the bridge were processed, revealing some challenges that such a monitoring system might encounter.

The numerical investigations reveal that both local and global damage in post-tensioned systems cause variations in static and quasi-static responses. The extent of variations in strain signals is influenced by the severity of the damage, such as the number of tendons affected and the extent of voids, as well as the sensor's proximity to the damage. The study also assessed the sensitivity of vertical displacement measurements to damage, confirming that strain generally offers greater sensitivity. However, it is challenging to draw broad conclusions since the results and sensitivity to damage vary based on the structure’s specifics. Different sensor locations show different sensitivities to damage, and the extent of the damage uniquely impacts each location. While the greatest variations typically occur when the damage is near the sensor, the trends and magnitudes of these changes differ across sensors. Therefore, this work confirms that damages in the post-tensioning induce detectable changes in sensor responses. In fact, these changes may be more sensitive to damage than traditional modal properties, offering an alternative approach for damage detection and monitoring. However, this study cannot definitively ascertain whether these changes would be detectable under normal operational conditions.

Under normal operational conditions, structural responses are significantly influenced by ambient conditions, primarily temperature. In this work, the impact of temperature was the main focus, but other factors such as solar irradiation, wind, and relative humidity also contribute to variations in structural responses. To effectively use continuously monitored bridge responses for damage detection, it is essential to compensate for these ambient variations. This report addressed temperature effects heuristically by identifying underlying trends in strain signals. Additionally, the potential of machine learning (ML) was explored to discern sudden changes in prestressing force from temperature variations. Initial ML results indicate that suitable ML procedures could identify such changes; however, further research is necessary to refine these methods and ensure accurate correction for ambient influences.

To enhance ML performance and achieve effective temperature compensation, more detailed and continuous data on ambient loading conditions are desired. The implementation of an SHM system could benefit from additional weather data, such as temperature, humidity, wind, and cloud cover, gathered directly on the bridge or from a nearby weather station. This additional data would support the development of ML models capable of distinguishing structural changes due to damage from those caused by environmental factors, thereby improving the reliability of SHM systems.

The analysis of signals measured on the Herøysund Bridge reveals indications of non-linear relationships under normal traffic loads, which can primarily be attributed to the non-linear behaviour inherent in a cracked prestressed concrete structure. Also, the effect of temperature on strain signals shows variability across different sensors, complicating the understanding of temperature-strain interactions. Initially, it was hypothesized that sensors located on the north beam exhibited a stronger non-linear relationship with temperature. However, further examination of strain values recorded by newly installed sensors indicates that this non-linear

temperature dependency is also present in sensors positioned on the south beam. These findings highlight the complexity of load and temperature dependency in the structural responses of the Herøysund Bridge, emphasizing the need for comprehensive strategies to account for these non-linearities in structural health monitoring systems.

Nevertheless, this study demonstrates the feasibility of extending structural health monitoring systems to function as truck weighing systems. For the Herøysund Bridge, this proved particularly challenging due to its unique structural circumstances and the limitations of the methods used. Despite these challenges, reasonable estimates of Gross Vehicle Weight (GVW) for heavy trucks were obtained. Better results may be achievable with other bridges, providing valuable data for generating local traffic models, updating numerical bridge models, and improving bridge assessment procedures. This highlights the potential of adapting existing infrastructure to deliver critical data for traffic monitoring and bridge maintenance, even when faced with complex structural and operational challenges.

Regarding the hardware and practical considerations of the monitoring system, this study shows that strain sensors attached to carbon fibre plates provide reliable readings for structural monitoring. Also it shows that, continuous monitoring systems must be robust and capable of enduring environmental conditions to ensure consistent data collection over time. Real-time access through online solutions is advantageous for continuous data analysis and prompt anomaly detection, while maintaining physical access to sensors is desirable for direct inspection and repair of any malfunctions, ensuring the system's reliability and longevity.

This work highlights the need for further research, particularly to understand the mechanisms of tendon failure and its impact on structural integrity. Key areas of investigation include the speed at which tendons break and the potential signatures these failures leave in recorded signals. Additionally, more studies are required to examine how voids and poor grout influence the extent of damage and to explore the effects of such damage on measurable load responses.

References

[1] A. Hagen and T. M. Andersen, "Asset management, condition monitoring and Digital Twins: damage detection and virtual inspection on a reinforced concrete bridge," *Structure and Infrastructure Engineering*, Feb. 2024, DOI: 10.1080/15732479.2024.2311911.

[2] E. Hamed and Y. Frostig, "Natural frequencies of bonded and unbonded prestressed beams–prestress force effects," *Journal of Sound and Vibration*, vol. 295, no. 1-2, pp. 28–39, Jul. 2006, DOI: 10.1016/j.jsv.2005.11.015.

[3] M. P. Limongelli et al., "Damage detection in a post-tensioned concrete beam – Experimental investigation," presented at the 5th European Workshop on Structural Health Monitoring, Sorrento, Italy, Jun. 2010.

[4] M. Selmurzaev, A. H. Andersson, and F. Hobbel, "Instrumentation report for Herøysund Bridge with additional channels – Strain gauge installation," HBM report, May 2023.

[5] HBK, "catman – Universal data acquisition and analysis software – Data sheet," accessed Jan. 7, 2025. [Online].
Available: https://www.hbm.com/fileadmin/mediapool/hbmdoc/technical/B04486.pdf

[6] L. Bohmann, *APReader* (Version 1.1.2) [Computer software], Sep. 2023. Available: https://github.com/leonbohmann/APReader, DOI: 10.5281/zenodo.8369804.

[7] D. Cantero and C. W. Kim, "Convoluted Reciprocity and Other Methods for Vehicle Speed Estimation in Bridge Weigh-in-Motion Systems," *Journal of Bridge Engineering*, vol. 29, no. 2, Feb. 2024, doi: 10.1061/JBENF2.BEENG-6422.

[8] J. Kalin, A. Žnidarič, and I. Lavrič, "Practical implementation of nothing-on-the-road bridge weigh-in-motion system," presented at the 9th International Symposium on Heavy Vehicle Weights and Dimensions, State College, PA, Aug. 2006.

[9] E. J. O'Brien, M. Quilligan, and R. Karoumi, "Calculating an Influence Line from Direct Measurements," *Proceedings of the Institution of Civil Engineers - Bridge Engineering*, vol. 159, no. 1, pp. 31–34, Feb. 2006, DOI: 10.1680/bren.2006.159.1.31.

[10] G. T. Frøseth, A. Rønnquist, D. Cantero, and O. Øiseth, "Influence line extraction by deconvolution in the frequency domain," *Computers and Structures*, vol. 189, pp. 21–30, Sep. 2017, DOI: 10.1016/j.compstruc.2017.04.014.

[11] T. Ojio, K. Yamada, and H. Shinkai, "BWIM systems using truss bridges," in *Bridge Management 4*, M. J. Ryall, G. A. R. Parke, and J. E. Harding, Eds. London, UK: Thomas Telford, 2000, pp. 434–441.

[12] S. Shi, M. Yarnold, S. Hurlebaus, and J. Mander, "Evaluation of a Load Cell-Based Bridge Weigh-in-Motion System," *Transportation Research Record*, vol. 2678, no. 1, pp. 1–15, Jan. 2024, DOI: 10.1177/03611981241263336

[13] Fédération Internationale du Béton (fib), *Structural Concrete: Textbook on Behaviour, Design and Performance*, 2nd ed., vol. 1. Lausanne, Switzerland: fib, 2009.

[14] S. M. Flatjord, "Model validation with measurements and effect of damage on strain signals," M.S. thesis, Dept. Structural Eng., Norwegian Univ. of Science and Technology, Trondheim, Norway, Jun. 2023. [Online]. Available: https://ntnuopen.ntnu.no/ntnu-xmlui/handle/11250/3093185

[15] A. Sveen, "Beregningsrapport - Herøysund bru, Bæreevneberegninger," Aas-Jakobsen, Oslo, Norway, 2020, unpublished.

[16] N. S. Eggum and M. Furnes, "Quantifying Structural Damage on the Herøysund Bridge through Strain and Displacement Response Analysis," M.S. thesis, Dept. Structural Eng., Norwegian Univ. of Science and Technology, Trondheim, Norway, Jun. 2024. [Online]. Available: https://ntnuopen.ntnu.no/ntnu-xmlui/handle/11250/3153539

[17] E. N. Husøy and E. H. Steen, "Machine learning-assisted structural health monitoring of Herøysund Bridge," M.S. thesis, Dept. Structural Eng., Norwegian Univ. of Science and Technology, Trondheim, Norway, Jun. 2024. [Online]. Available: https://ntnuopen.ntnu.no/ntnu-xmlui/handle/11250/3156765

[18] D. Cantero, "VBI-2D – Road vehicle-bridge interaction simulation tool and verification framework for Matlab," *SoftwareX*, vol. 26, 2024, DOI: 10.1016/j.softx.2024.101725

[19] M. Nwamma, "Review and application of optimal sensor placement method on Herøysund Bridge," M.S. thesis, Dept. Computer Science and Computational Engineering, UiT The Arctic Univ. of Norway, Tromsø, Norway, May 2023. [Online]. Available: https://munin.uit.no/handle/10037/34263

[20] P. N. Berg, "Beam based finite element modelling of Herøysund Bridge," M.S. thesis, Dept. Structural Eng., UiT The Arctic Univ. of Norway, Tromsø, Norway, May 2023. [Online]. Available: https://munin.uit.no/handle/10037/31344

[21] A. Gonilovic and S. S. Løken, "Capacity analysis of Herøysund Bridge with a damaged post-tensioned system," M.S. thesis, Dept. Structural Eng., Norwegian Univ. of Science and Technology, Trondheim, Norway, Jun. 2023. [Online]. Available: https://ntnuopen.ntnu.no/ntnu-xmlui/handle/11250/3093190

[22] D. Cantero and A. González, "Bridge damage detection using weigh-in-motion technology," *ASCE Journal of Bridge Engineering*, vol. 20, no. 5, May 2017, DOI: 10.1061/(ASCE)BE.1943-5592.0000674

NTNU

Norwegian University of
Science and Technology